



RESEARCH ARTICLE

Microsomal prostaglandin E synthase-1 is involved in the metabolic and cardiovascular alterations associated with obesity

Constanza Ballesteros-Martínez¹ | Raquel Rodrigues-Díez^{1,2}  | Luis M. Beltrán^{3,4} | Rosa Moreno-Carriles⁵ | Ernesto Martínez-Martínez⁶ | María González-Amor^{1,2} | Jose Martínez-González^{2,7} | Cristina Rodríguez^{2,8} | Victoria Cachofeiro^{2,6} | Mercedes Salaices^{1,2} | Ana M. Briones^{1,2} 

¹Departamento de Farmacología, Facultad de Medicina, Universidad Autónoma de Madrid, Instituto de Investigación Hospital Universitario La Paz (IdiPaz), Madrid, Spain

²CIBER de Enfermedades Cardiovasculares, ISCIII, Madrid, Spain

³Servicio de Medicina Interna, Hospital Universitario La Paz, IdiPaz, Madrid, Spain

⁴Servicio de Medicina Interna, Hospital Virgen del Rocío - IBI Sevilla, Departamento de Medicina, Universidad de Sevilla, Sevilla, Spain

⁵Servicio de Angiología y Cirugía vascular, Hospital Universitario La Princesa, Madrid, Spain

⁶Departamento de Fisiología, Facultad de Medicina, Universidad Complutense de Madrid, Instituto de Investigación Sanitaria Gregorio Marañón (IISGM), Madrid, Spain

⁷Instituto de Investigaciones Biomédicas de Barcelona (IIBB-CSIC), Instituto de Investigación Biomédica (IIB) Sant Pau, Barcelona, Spain

⁸Institut de Recerca Hospital de la Santa Creu i Sant Pau (IRHSCSP), IIB-Sant Pau, Barcelona, Spain

Correspondence

Ana M. Briones, Departamento de Farmacología, Facultad de Medicina, Universidad Autónoma de Madrid, C/Arzobispo Morcillo 4, 28029 Madrid, Spain. Email: ana.briones@uam.es

Funding information

Ministerio Ciencia e Innovación. Programa Juan de la Cierva, Grant/Award Number: IJCI-2017-31399; Comunidad de Madrid, Grant/Award Number: B2017/BMD-3676 AORTASANA, FEDER-a way to build Europe; Fondo Europeo de Desarrollo Regional, Grant/Award Number: SAF2016-80305P; Ministerio de Ciencia e Innovación, Grant/Award Number: FIS PI18/0257

Background and Purpose: Microsomal prostaglandin E synthase-1 (mPGES-1) is an inducible isomerase responsible for prostaglandin E₂ production in inflammatory conditions. We evaluated the role of mPGES-1 in the development and the metabolic and cardiovascular alterations of obesity.

Experimental Approach: mPGES-1^{+/+} and mPGES-1^{-/-} mice were fed with normal or high fat diet (HFD, 60% fat). The glycaemic and lipid profile was evaluated by glucose and insulin tolerance tests and colorimetric assays. Vascular function, structure and mechanics were assessed by myography. Histological studies, q-RT-PCR, and western blot analyses were performed in adipose tissue depots and cardiovascular tissues. Gene expression in abdominal fat and perivascular adipose tissue (PVAT) from patients was correlated with vascular damage.

Abbreviations: AA, arachidonic acid; AAA, abdominal aortic aneurysm; BMI, body mass index; BP, blood pressure; CLS, crown-like structures; cPGES, cytosolic prostaglandin E synthase; DEA-NO, diethylamine NONOate; GTT, glucose tolerance test; HFD, high fat diet; IMT, intima media thickness; ITT, insulin tolerance test; KHS, Krebs-Henseleit solution; mPGES-1, microsomal prostaglandin E synthase-1; mPGES-2, microsomal prostaglandin E synthase-2; MRAs, mesenteric resistance arteries; PFA, paraformaldehyde; PLA₂, phospholipase A2; PVAT, perivascular adipose tissue; PWV, pulse wave velocity; WAT, white adipose tissue; WGA, wheat germ agglutinin.

Constanza Ballesteros-Martínez and Raquel Rodrigues-Díez contributed equally to this study.

This is an open access article under the terms of the Creative Commons Attribution-NonCommercial-NoDerivs License, which permits use and distribution in any medium, provided the original work is properly cited, the use is non-commercial and no modifications or adaptations are made.

© 2021 The Authors. *British Journal of Pharmacology* published by John Wiley & Sons Ltd on behalf of British Pharmacological Society.

Key Results: Male mPGES-1^{-/-} mice fed with HFD were protected against body weight gain and showed reduced adiposity, better glucose tolerance and insulin sensitivity, lipid levels and less white adipose tissue and PVAT inflammation and fibrosis, compared with mPGES-1^{+/+} mice. mPGES-1 knockdown prevented cardiomyocyte hypertrophy, cardiac fibrosis, endothelial dysfunction, aortic insulin resistance, and vascular inflammation and remodelling, induced by HFD. Obesity-induced weight gain and endothelial dysfunction of resistance arteries were ameliorated in female mPGES-1^{-/-} mice. In humans, we found a positive correlation between mPGES-1 expression in abdominal fat and vascular remodelling, vessel stiffness, and systolic blood pressure. In human PVAT, there was a positive correlation between mPGES-1 expression and inflammatory markers.

Conclusions and Implications: mPGES-1 inhibition might be a novel therapeutic approach to the management of obesity and the associated cardiovascular and metabolic alterations.

KEYWORDS

adipose tissue alterations, inflammation, mPGES-1, obesity, vascular function and remodelling

1 | INTRODUCTION

Obesity, particularly visceral obesity, is one of the major risk factors in the development of metabolic disorders such as Type 2 diabetes and insulin resistance (Vecchié et al., 2018). In normal conditions, adipose tissue participates in the maintenance of body homeostasis, including normal vascular structure and tone. However, dysfunctional obese adipose tissue is characterized by a proinflammatory status and secretion of proinflammatory mediators associated with the development of cardiovascular disease (Fuster et al., 2016; Vecchié et al., 2018).

In physiological conditions, prostaglandin E₂ (PGE₂) is synthesized from tissue phospholipids and arachidonic acid (AA) by the sequential effects of phospholipase A_{2α} (PLA_{2α}), cyclooxygenase (COX)-1, and two constitutive PGE₂ synthases (PGES): microsomal PGES (mPGES)-2 and cytosolic PGES (cPGES). However, in inflammatory conditions, inducible COX-2 and mPGES-1 isomerase are the main enzymes involved in the biosynthesis of PGE₂ (Koeberle & Werz, 2015; Samuelsson et al., 2007). PGE₂ is one of the most abundant prostanoids released by adipose tissue (Fain et al., 2002) and there is increasing evidence that PGE₂ affects adipogenesis and has anti-lipolytic effects (García-Alonso & Clària, 2014), thus promoting the enlargement of fat depots. Moreover, preadipocytes release proinflammatory mediators in a PLA₂/PGE₂ dependent manner (Leiguez et al., 2020). However, studies evaluating changes in PGE₂ levels or in enzymes involved in PGE₂ synthesis in adipose tissues in obesity have reported conflicting results. Thus, Héту and Riendeau (2007) found significantly decreased levels of PGE₂ in subcutaneous and inguinal white adipose tissue (WAT) in murine obesity, whereas other authors found augmented PGE₂ levels in isolated adipocytes from obese rats (Chan et al., 2016) or in human obese WAT (García-Alonso et al., 2016). Importantly, mice lacking PLA_{2α}

What is already known

- mPGES-1 deficiency prevents obesity-induced weight gain.

What does this study add

- mPGES-1 deficiency prevents obesity-induced metabolic and cardiovascular alterations.
- In humans, mPGES-1 positively correlates with inflammation and vascular damage.

What is the clinical significance

- mPGES-1 inhibition could prevent obesity-induced metabolic and vascular alterations.
- mPGES-1 inhibitors might be a safe therapeutic tool in obese patients.

(Jaworski et al., 2009), COX-2 (Fain et al., 2001; Ghoshal et al., 2011), or mPGES-1 (Pierre et al., 2018) are protected against body weight gain, adipose tissue enlargement, and/or inflammation induced by a high fat diet (HFD). On the other hand, no differences in gain weight following mPGES-1 deletion have been described in animals fed a modified HFD containing a lower amount of fat for shorter times

(Sasaki et al., 2021). Of note, the contribution of mPGES-1 to glucose and lipid metabolism in obesity has been less explored.

In addition to metabolic alterations, obesity is associated with cardiovascular complications such as endothelial dysfunction, thickened vascular wall, increased vascular stiffness, and cardiac hypertrophy and fibrosis (Briones et al., 2014; Martínez-Martínez et al., 2015; Prieto et al., 2014) that clearly contribute to enhance cardiovascular risk. Different factors are involved in the cardiovascular alterations associated with obesity. Specifically, the participation of prostanoids derived from COX-2 in the functional vascular alterations induced by obesity has been demonstrated (Briones et al., 2014; Even et al., 2014; Muñoz et al., 2015; Prieto et al., 2014; Vessières et al., 2010). However, the contribution of mPGES-1 to the cardiovascular alterations associated to obesity is currently unknown.

We hypothesized that in obesity, there is an inflammatory process mediated by mPGES-1-derived prostanoids that contributes to the structural and functional cardiovascular alterations and to the metabolic changes associated with this pathology. We performed studies in a model of obesity in mPGES-1 knockout mice and in humans.

2 | METHODS

2.1 | Human studies

These studies were conducted according to the principles of the Declaration of Helsinki and approved by the Institutional Research Ethics Committees of Hospital Universitario La Paz (PI-1747) and Hospital Universitario La Princesa (PI-825) (Madrid, Spain). All subjects were aware of the research nature of the study and gave informed consent. Abdominal adipose tissue was obtained from patients during abdominal surgery in the Hepatobiliary Surgery Unit of the Hospital La Paz and the vascular study was carried out in the Cardiovascular Unit in the same hospital. Patients (18- to 75-years-old) scheduled for elective abdominal surgery were offered to participate in the study. Exclusion criteria included inflammatory and neoplastic conditions, active smoking, or use of recreational drugs, established cardiovascular disease and pregnancy. Recruited patients were subjected to complete anamnesis, physical examination, and blood pressure (BP), pulse wave velocity (PWV), and intima media thickness (IMT) measurements. BP was determined using an automatic oscillometric device OMRON-M3 (HEM-7200-E-Omron Healthcare, Kyoto, Japan) according to international guidelines recommendations (Mancia et al., 2013). PWV was determined by applanation tonometry using SphygmoCor device (AtCor Medical, Australia). IMT was measured according to international consensus recommendations (Touboul et al., 2012) using a Mylab Seven system (Esaote, Genova, Italy) with a 4- to 13-MHz probe. The system employed a dedicated software radiofrequency-tracking technology to obtain IMT (QIMT[®]) (Dan et al., 2011). The characteristics of the patients studied are summarized in Table S1.

Perivascular adipose tissue (PVAT) was obtained from patients undergoing open surgery for abdominal aortic aneurysm (AAA) in the

Angiology and Vascular Surgery Unit of the Hospital La Princesa. Inclusion criteria include patients with an AAA ≥ 5.5 cm (≥ 5 cm in women) in diameter, proven by imaging technique, symptomatic or asymptomatic, or those who during the follow-up would have experienced rapid growth (more than 0.5 cm in a 6-month interval) and that met the criteria for open surgery. Exclusion criteria include inflammatory aneurysm, active neoplastic conditions, HIV positive serology and pregnancy. Characteristics of the studied population are included in Table S2. Both abdominal and aortic adipose tissue were frozen at -80°C for qRT-PCR analysis.

2.2 | Animal models

All experimental procedures and animal care were approved by the Ethical Committee of Research of the Universidad Autónoma de Madrid (UAM) and Dirección General de Medio Ambiente, Comunidad de Madrid, Spain (PROEX 345/14, PROEX 183.2/20), and conducted in accordance with the current Spanish and European Policy for Animal Protection RD53/2013. The experiments were conducted in accordance with the National Institutes of Health (NIH) Guide for the Care and Use of Laboratory Animals and the ARRIVE (Percie du Sert et al., 2020) and BJP guidelines (Lilley et al., 2020).

mPGES-1^{-/-} mice and their wild-type littermates (mPGES-1^{+/+}) on C57BL/6J background were generated by crossing heterozygous knockout males in DBA genetic background kindly donated by Pfizer with wild-type females on C57BL/6J background, bred at the Animal Care Facility of the Faculty of Medicine, UAM, for 11 generations.

Two-month-old male and female mPGES-1^{+/+} and mPGES-1^{-/-} mice were randomly divided in two groups: Control, fed with a standard diet (5LF2* EURodent Diet, 6.6% kcal from fat, LabDiet, USA); and obese, fed with high fat diet (HFD) (TD.06414, 60.3% kcal from fat, ENVIGO, USA) for 13 weeks. This HFD model has been selected based on previous studies as it reproduces some of the features of human obesity (Buettner et al., 2007; Wang & Liao, 2012).

Animals were randomly distributed in the different experimental groups with each group having the same number of animals by design. We did not utilize statistical methods to predetermine sample or group sizes, and the number of animals used was estimated from our previous experience with this animal model. Investigators for outcome assessments were not blinded to group allocation unless specified. All mice were bred at the conventional Animal Care Facility of the Faculty of Medicine, Universidad Autónoma de Madrid (UAM) under controlled conditions at 25°C in a 12-h light/dark cycle, with ad libitum access to water and food. Animals were housed in groups of two or four in standard polypropylene cages containing rich bedding made of dried wood chips.

Mice were weighed weekly. Blood pressure was measured by tail-cuff plethysmography at the end of the procedure after previous training; eight individual observations per animal were performed and averaged. All the measurements were made at the same time of the day. The animal study complied with the 3Rs.

2.3 | Tissue preparation

Mice were killed by CO₂ narcosis. Aorta and first-order branches of the mesenteric artery were cleaned and placed in cold (4°C) Krebs–Henseleit solution (KHS) (in mmol·L⁻¹) (115 NaCl, 25 NaHCO₃, 4.7 KCl, 1.2 MgSO₄·7H₂O, 2.5 CaCl₂, 1.2 KH₂PO₄, 11.1 glucose, and 0.01 Na₂EDTA) bubbled with a 95% O₂–5% CO₂ mixture (pH = 7.4). Segments of aorta and mesenteric arteries were immediately used for functional, structural, or mechanical studies using wire or pressure myography or immediately frozen and stored at –80°C.

Aortic PVAT was also removed and frozen at –80°C for qPCR analysis. WAT and perirenal adipose tissue were cleaned, weighed and frozen at –80°C or fixed in 4% paraformaldehyde (PFA, pH = 7.4) and kept at 4°C for histological studies. Adiposity index (%) was calculated: [(abdominal + perirenal fat pads)/(final body weight – sum of abdominal and perirenal fat pads) × 100].

Left cardiac ventricles were isolated, weighed, and frozen at –80°C or fixed in 4% PFA and kept at 4°C for histological studies. Cardiac hypertrophy was calculated as the left ventricle weight normalized by the tibia length.

2.4 | Insulin and glucose tolerance tests

The glycaemic profile was studied 2 weeks before the end of the experiment. Mice were fasted 4 h for the insulin tolerance test (ITT) and 16 h for the glucose tolerance test (GTT). Animals were weighed and basal glucose levels were measured. Then, **insulin** (Insulin Actrapid 100 UI/ml, NOVO NORDISK, 0.8 UI/Kg of mouse) or hypertonic glucose solution (10%, Fresenius Kabi, 20 µl·kg⁻¹ of mouse) were injected i.p.. Glycaemia was measured from tail blood at different time points (15, 30, 60, 90, and 120 min) using a standard glucometer (FreeStyle Optium).

2.5 | Measurement of lipid levels

Total cholesterol (Ref. 1001091, SpinReact), triglycerides (Ref. 1001313, SpinReact), LDL-Cholesterol-D (Ref. 41023, SpinReact) and oxLDL (Ref. ab242301, Abcam) levels were evaluated in plasma samples following manufacturers' instructions.

2.6 | Histological studies

PFA fixed tissue samples were dehydrated, embedded in paraffin, and cut in 5 µm-thick sections. Then, sections were deparaffinized and hydrated (5 min Xilol, 5 min EtOH 100%, 5 min EtOH 70%, 5 min H₂O) for further analysis. All stains were coverslipped with DPX mounting medium.

WAT sections were stained with haematoxylin and eosin to measure adipocyte size and number. After rehydration, samples were

incubated with haematoxylin for 4 min, washed and stained with eosin for 5 min. For each mouse, 3 images of adipose tissue were taken and analysed using ImageJ software (ImageJ, NIH, Bethesda, MD, USA, RRID:SCR_001935). Images were duplicated and calibrated. Background was subtracted, and the excess of noise was removed. A threshold was applied to the images which were then converted to binary format. Borders of adipocytes were enhanced and adipocytes with broken membranes were separated manually with the “cut drawing” tool. Finally, adipocytes area was measured as described (Parlee et al., 2014). Data analysis was carried out with the average of the images of each mouse.

Aortic rings were stained with haematoxylin and eosin as described above to determine aortic structure. Vessel internal and external perimeter (Pi, Pe) were measured using ImageJ Software (ImageJ, NIH). Cross-sectional area (CSA) was calculated as $CSA = (Pe^2 - Pi^2) / 4\pi$. Results were quantified without knowledge of the sample treatments.

Cardiac, WAT and aorta sections were stained with Picrosirius red to detect collagen fibres. Sections were incubated 2 min with picric acid and washed. Then, they were stained with Sirius red solution for 1 h and dehydrated. The area of cardiac interstitial fibrosis was identified as the ratio of interstitial fibrosis to the total tissue area after excluding vessel areas from the region of interest. For each mouse, 5 fields of two different sections were analysed and averaged. In adipose tissue samples, the area of pericellular fibrosis was identified as the ratio of collagen deposition to the total tissue area after excluding vessels area from the region of interest. This value was normalized by the number of adipocytes. For each sample, 10–15 fields were analysed using a 40 × objective (Leica DM 2000; Leica Camera AG, Wetzlar, Germany) and quantified (Leica Q550 IWB; Leica Camera AG) and averaged. In aorta, images were captured using an Olympus BX50 microscope at 10× magnification. The percentage of fibrosis was determined as the ratio between collagen area in the media and the total medial area. Results were quantified without knowledge of the sample treatments.

Mean cardiomyocyte area was evaluated in Wheat Germ Agglutinin (WGA)-stained cardiac sections. Tissue sections were incubated in a wet chamber with WGA-CY3 (5 µg·ml⁻¹, Biotium) and Hoechst 33342 (0.01 mg·ml⁻¹, ThermoFisher) in PBS-Tween (PBS-T, 0.05%), during 1 h at room temperature. Samples were washed with PBS-T, covered-slipped using Prolong and kept at 4°C. Three stacks per animal were captured with a confocal microscope (Leica TCS SP5, Leica Microsystems) and individual projections were reconstructed. At least 30 cardiomyocytes in each field were measured using Metamorph Image Analysis Software (Molecular Devices Corp. Downingtown, PA, USA, RRID:SCR_002368) and averaged.

2.7 | Immunohistochemistry studies

Immunohistochemistry was performed in 5 µm thick paraffined WAT sections to detect macrophage infiltration. After de-waxing, antigen retrieval was performed using Proteinase-K method by incubation

with Proteinase-K (Roche, 20 mg·ml⁻¹ in Tris-acetato-EDTA buffer) for 3 min and washed with PBS-Tween (PBS-T, 0.5%). Endogenous peroxidase activity was blocked by 10% H₂O₂ (Panreac, 10 min). Free protein binding sites were blocked with 2% fetal bovine serum (FBS, Sigma, 1 h). Then, samples were incubated overnight with a rat primary antibody against mouse F4/80 (clone Cl:A3-1. Bio-Rad Cat# MCA497RT, RRID:AB_1102558, 1/100). Samples were washed with PBS-T and incubated with a secondary HRP-conjugated anti-rat antibody (Millipore Cat# AP136P, RRID:AB_11214444) for 1 h. HRP activity was visualized using diaminobenzidine (VectorLab) as substrate. Sections were counterstained with haematoxylin, dehydrated and mounted in DPX mounting medium. Crown-like structures (CLS) were defined in the sections as single and entire dead adipocytes, partly or totally encircled by macrophages.

2.8 | Vascular function

Reactivity of mouse aorta and mesenteric resistance arteries was studied in a wire myograph (Danish Myo Tech, Aarhus, Denmark). After a 30-min equilibration period in oxygenated KHS, arterial segments were stretched to their optimal lumen diameter for active tension development. Contractility of segments was tested by an initial exposure to a high-K⁺ solution (K⁺-KHS, 120 mmol·L⁻¹). Arteries were discarded if K⁺-KHS response was lower than 0.5 mN·mm⁻¹. Concentration–response curves to **acetylcholine** (1 nmol·L⁻¹ to 30 μmol·L⁻¹), insulin (10 nmol·L⁻¹ to 30 μmol·L⁻¹), or the NO donor diethylamine NONOate (DEA-NO, 10 nmol·L⁻¹ to 30 μmol·L⁻¹) were obtained after precontraction with phenylephrine. To minimize variation, vasodilator responses were expressed as the percentage of relaxation of the tone induced by phenylephrine.

2.9 | Pressure myography

The mechanical and structural properties of mesenteric arteries were studied with a pressure myograph (Danish Myo Tech, Aarhus, Denmark). PVAT-free vessels were mounted on two glass microcannulae, set to a pressure of 45 mmHg and equilibrated for 30 min at 37°C in calcium-free KHS (0 mM Ca²⁺; omitting calcium and adding 1 mmol·L⁻¹ EGTA). A pressure-diameter curve was obtained by increasing intraluminal pressure in 20 mmHg steps from 3 to 120 mmHg. Every intraluminal pressure was maintained for 2 min. Internal and external diameters were measured under passive conditions ($D_{iO_{Ca}}$, $D_{eO_{Ca}}$) at each intraluminal pressure using ImageJ software.

2.10 | Calculation of passive mechanical and structural parameters

Structural and mechanical parameters were calculated as follows:

$$\text{Wall thickness (WT)} = (D_{eO_{Ca}} - D_{iO_{Ca}}) / 2;$$

$$\text{wall : lumen} = (D_{eO_{Ca}} - D_{iO_{Ca}}) / 2D_{iO_{Ca}}.$$

Circumferential wall strain (ϵ) = $(D_{iO_{Ca}} - D_{00Ca}) / D_{00Ca}$, where D_{00Ca} is the internal diameter at 3 mmHg and $D_{iO_{Ca}}$ is the observed internal diameter for a given intravascular pressure both measured in OCa²⁺ medium. Circumferential wall stress (σ) = $(P \times D_{iO_{Ca}}) / (2WT)$, where P is the intraluminal pressure (1 mmHg = 1.334×10^3 dynes·cm⁻²) and WT is the wall thickness at each intraluminal pressure in OCa²⁺-KHS. Incremental distensibility represents the percentage of change in the arterial internal diameter for each interval change in intraluminal pressure, and was calculated as follows:

$$\text{Incremental distensibility} = \Delta D_{iO_{Ca}} / (D_{iO_{Ca}} \times \Delta P) \times 100.$$

The arterial stiffness independent of the geometry was determined by Young's elastic modulus (E = stress/strain). The stress–strain relationship is nonlinear; therefore, it is more appropriate to obtain a tangential or incremental elastic modulus (E_{inc}) by determining the slope of the stress–strain curve ($E_{inc} = \delta\sigma / \delta\epsilon$). E_{inc} was obtained by fitting the stress–strain data from each animal to an exponential curve using the equation: $\sigma = \sigma_{orig} e^{\beta\epsilon}$, where σ_{orig} is the stress at the original diameter (diameter at 3 mmHg). Taking derivatives of the equation, we determined that $E_{inc} = \beta\sigma$. For a given σ -value, E_{inc} is directly proportional to β . An increase in β implies an increase in E_{inc} , which indicates an increase in stiffness.

2.11 | Organization of internal elastic lamina

The 3D structure of the internal elastic lamina of mesenteric arteries pressure-fixed at 45 mmHg was studied using fluorescence confocal microscopy (Leica TCS SP5, Leica Microsystems) based on the auto-fluorescent properties of elastin (Ex 488 nm and Em 500–560 nm). Serial optical sections were captured from the adventitia to the lumen (z step = 0.5 μm) using a X63 oil objective (Zoom 4). At least four stacks of images from different regions per artery were taken. From each stack of images, individual projections of the internal elastic lamina were reconstructed and mean fenestrae area and number were calculated taking into account the luminal surface area occupied by the internal elastic lamina in a 1-mm length segment.

2.12 | RT-PCR assay

Total RNA was obtained with TRI Reagent[®] (Sigma-Aldrich); 1 μg was reversed transcribed to cDNA with NZY First-Strand cDNA Synthesis Kit (Nzytech). Quantitative PCR (qPCR) was performed in a 7500 Fast ABI System (Invitrogen Life Technologies) in duplicate to ensure the reliability of qRT-PCR values, using specific q-PCRs probes and assays (Table S3). Data were analysed using the average of the duplicate values. β_2 -microglobulin, ribosomal protein large P0, or 18 s were used

as calibrators. PCR cycle programmes were as follows: initial denaturation (30 s, 95°C), followed by 40 cycles (95°C, 5 s and 60°C, 30 s). Melting curve was performed in SYBR green reactions to show PCR product specificity. To calculate the relative index of gene expression, we employed the $2^{-\Delta\Delta C_t}$ method. mRNA expression in mice was normalized against mPGE₂-1^{+/+} control samples to minimize variation. For human samples, mRNA expression is expressed as Log ($2^{-\Delta\Delta C_t}$) of the corresponding gene after normalization with its calibrator.

2.13 | Lipid peroxidation

Lipid peroxidation in frozen segments of aorta and heart was determined using a lipid peroxidation (malondialdehyde) assay kit (ab118970, Abcam) following the manufacturer's instructions.

2.14 | PGE₂ levels

PGE₂ levels were determined in frozen segments of aorta and heart using the PGE₂ ELISA Kit – Monoclonal (No. 514010, Cayman). Samples were homogenized (0.1-mol·L⁻¹ phosphate, pH 7.4, 1mmol·L⁻¹ EDTA) with a Dounce homogenizer. The assay was performed following the manufacturer's instructions. PGE₂ concentrations were calculated as the amount of PGE₂ per microgram of protein.

2.15 | Western blot analysis

Total protein from the left ventricle were obtained with TRI Reagent® (Sigma-Aldrich) following the manufacturer's instructions. Cardiac proteins were separated by SDS-PAGE and transferred to Hybond-c Extra nitrocellulose membranes (Hybond-P; Amersham Biosciences, Piscataway, NJ) with the Trans-Blot Turbo Transfer System (Bio.Rad). Membranes were probed overnight with primary antibodies for TGF-β (Abcam, Ref. ab19053, RRID:AB_778340, 1/1000), α-smooth muscle actin (α-SMA, GeneTex, Ref. GTX100034, RRID:AB_1240408, 1/250), and GAPDH (Cell Signaling Technology Cat# 8884, RRID: AB_11129865, 1:5000) that was used as a loading control. Secondary antibodies were incubated for 1 h. Signals were detected using the ECL system (Amersham Pharmacia Biotech). Results are expressed as an n-fold increase over the values of the control group in densitometric arbitrary units, to minimize variation.

2.16 | Data and statistical analysis

The data and statistical analysis in this study complied with the recommendations on experimental design and analysis in pharmacology (Curtis et al., 2018). Data are expressed as mean ± SEM of the number of animals or patients studied. Data are reported as dot plots that represent different biological replicates. When this is not possible, the number of animals (n) is reported in figures or figure legends. The

declared group size is the number of these biological replicates, and statistical analysis was performed using these independent values. Statistical analysis was undertaken only for studies in which each group size was at least $n = 5$. In some experiments, group sizes became unequal during the study owing to biological loss (i.e., death of the mouse), technical failure, undetectable expression or presence of outliers that were excluded using predefined criteria. The ROUT method was used to exclude data from the analysis. After Shapiro-Wilk normality test to determine data distribution, differences between groups were determined by one-way or two-way ANOVA or its corresponding non-parametric test (Kruskal-Wallis) attending to the normal distribution of the samples, followed by Bonferroni's or Dunn's post hoc test when appropriate. In human studies, gene expression was log-transformed to obtain a normal distribution. Correlations were assessed using Spearman's correlation tests. Data were analysed with the GRAPHPAD PRISM 7 software (Graphpad Software, Inc., San Diego, CA, USA. RRID:SCR_002798). $P < 0.05$ was considered significant.

2.17 | Materials

All drugs were dissolved in distilled water and purchased from Sigma-Aldrich (Madrid, Spain), unless otherwise specified. Primary antibodies used were supplied as follows: TGF-β, Abcam, Ref. ab190503, 1/1000), α-SMA, GeneTex, Ref. GTX100034, 1/250), GAPDH (Cell Signaling Technology Cat# 8884, Ref: D16H11, 1/5000) and F4/80 (Bio-Rad Cat# MCA497, clone Cl:A3-1. AbD Serotec, 1/100).

2.18 | Nomenclature of targets and ligands

Key protein targets and ligands in this article are hyperlinked to corresponding entries in the IUPHAR/BPS Guide to PHARMACOLOGY (<http://www.guidetopharmacology.org>) and are permanently archived in the Concise Guide to PHARMACOLOGY 2021/22 (Alexander, Christopoulos et al., 2021; Alexander, Cidlowski et al., 2021; Alexander, Fabbro et al., 2021; Alexander, Kelly et al., 2021).

3 | RESULTS

3.1 | mPGE₂-1 deficiency protects against body weight gain and improves the adverse glycaemic and lipid profile induced by a HFD

In males given the HFD, *Ptges* mRNA levels did not change in WAT, PVAT, aorta, or heart, although a tendency to decrease was observed in WAT (Figure S1A). PGE₂ levels were not changed, either by diet or genotype in aorta or heart (Figure S1B,C).

mPGE₂-1^{-/-} mice fed on normal diet gained similar weight over the course of the experiment and had similar basal glycemia, glucose

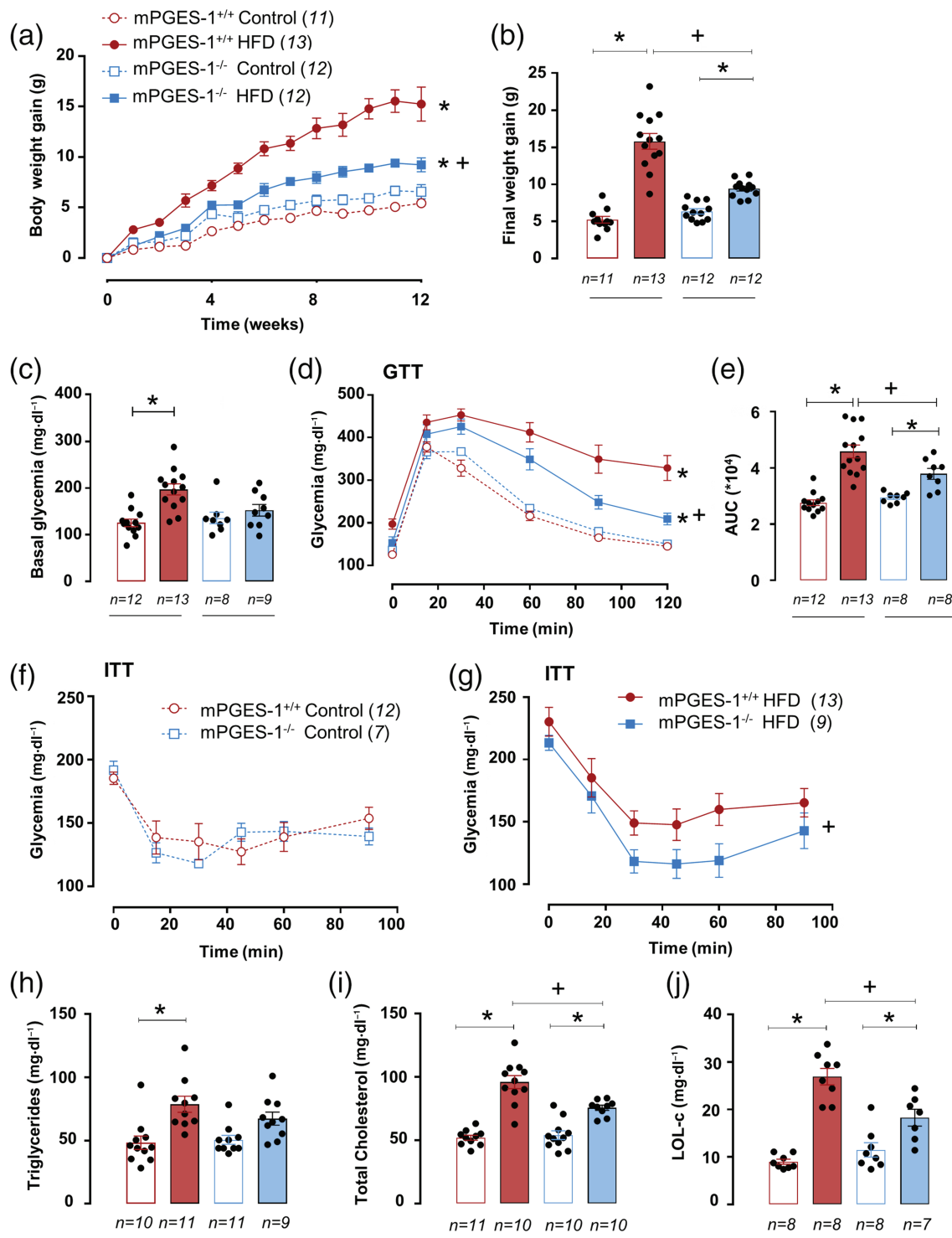


FIGURE 1 mPGES-1 deficiency protects against high fat diet (HFD)-induced body weight gain and improves the glycaemic and lipid profiles. (a,b) Body weight gain, (c) basal glucose levels, (d) glucose tolerance test (GTT), (e) area under the curve (AUC) of GTT, and (f,g) insulin tolerance test (ITT), in mPGES-1^{+/+} and mPGES-1^{-/-} mice fed with normal diet (control) and HFD. (h–j) Triglycerides, total cholesterol, and LDL-cholesterol levels in plasma samples of mice from all experimental groups. In bar graphs, each dot represents one mouse. Data shown are means ± SEM, with individual values in (b,c,e,h–j). **P* < 0.05, significantly different from control of each genotype. †*P* < 0.05, significantly different from mPGES-1^{+/+} under the same diet; one-way (b,c,e,h–j) or two-way ANOVA (a,d,f,g) or non-parametric Kruskal–Wallis test. The number of animals in each group is shown in parentheses or below each bar

tolerance and insulin sensitivity and lipid levels that were similar to those in mPGES-1^{+/+} mice (Figure 1). mPGES-1 gene deletion partly prevented the increase in body weight gain in HFD-fed animals, compared with wild-type littermates (Figure 1a,b). These effects were accompanied by an improvement in basal glycaemia, glucose tolerance, insulin sensitivity, and lipid levels in obese animals (Figure 1c–j), without significant changes in plasma oxLDL (mPGES-1^{+/+} Control: 0.015 ± 0.003; mPGES-1^{+/+} HFD: 0.013 ± 0.004; mPGES-1^{-/-} Control: 0.020 ± 0.002; mPGES-1^{-/-} HFD: 0.019 ± 0.003 μg·ml⁻¹, *n* = 6 all groups).

3.2 | mPGES-1 deficiency protects against HFD-induced adiposity, fibrosis, and macrophage infiltration

mPGES-1 knockdown did not affect the weight of adipose tissues in male mice fed on normal diet (Table S4). However, HFD did increase the perirenal and the abdominal adipose tissue weight, and adiposity index, more in mPGES-1^{+/+} than in mPGES-1^{-/-} mice (Table S4). Adipocyte size and collagen deposition in WAT was similar in mPGES-1^{-/-} and mPGES-1^{+/+} mice fed on normal diet (Figure 2a,b). HFD increased adipocyte size and adipose tissue fibrosis in mPGES-1^{+/+} mice, but not in mPGES-1^{-/-} mice (Figure 2a,b).

No differences in the expression of *Lep*, *Adipoq*, *Pparg*, or macrophage markers *Ccl2* and *Adgre1* expression or CLS presence were observed between genotypes in mice fed on normal diet (Figure 2c–e, g–i). Strikingly, mPGES-1 knockdown increased basal *Tnfa* expression (Figure 2f). HFD increased *Lep* mRNA in WAT from mPGES-1^{+/+} but not in knockout mice (Figure 2c). Conversely, the HFD-induced adiponectin expression was greater in mPGES-1^{-/-} than in mPGES-1^{+/+} mice (Figure 2d). *Pparg* expression was similarly augmented by the HFD in both groups (Figure 2e). HFD tended to increase *Tnfa* expression in mPGES-1^{+/+} animals whereas the opposite was observed in knockout mice (Figure 2f). Finally, HFD increased expression of *Ccl2* and the macrophage marker *Adgre1* and the presence of CLS in mPGES-1^{+/+} mice, but not in mPGES-1^{-/-} mice (Figure 2g–i).

3.3 | mPGES-1 deficiency protects against HFD-induced endothelial dysfunction and vascular insulin resistance

Systolic blood pressure (SBP) was similar in all the experimental groups (Table S5). In male mice, HFD impaired endothelium-dependent vasorelaxation to acetylcholine and to insulin in aorta from mPGES-1^{+/+} but not in knockout mice (Figures 3a,b and S2). Similar results were observed in mesenteric resistance arteries (Figure 3e,f). No differences in vasodilator responses to DEA-NO were observed between groups, either in aorta (Figure 3c,d) or in mesenteric arteries (Figure 3g,h), thus excluding changes in vascular smooth muscle cells sensitivity to NO as responsible for the observed effects.

3.4 | mPGES-1 deficiency protects against HFD-induced vascular and PVAT inflammation

HFD increased aortic mRNA levels of several inflammatory genes such *Ccl2*, *Iil1b*, *Tnfa*, interferon stimulated gene 15 (*Isg15*), and those for NADPH oxidase 1, 2, and 4 (*Nox1*, *Cybb*, *Nox4*) in mPGES-1^{+/+} but not in mPGES-1^{-/-} mice (Figure 4a,b). Unexpectedly, under basal conditions, mPGES-1^{-/-} knockdown enhanced the expression of *Ccl2*, *Iil1b*, and *Nox1* (Figure 4a,b). No differences in MDA levels were observed in the four experimental groups (Figure 4c).

Given the importance of PVAT as a key location for accumulation of immune cells in obesity, we addressed the consequences of mPGES-1 deletion on the inflammatory profile of aortic PVAT. In agreement with results observed in WAT, mRNA levels of *Adgre1* and *Ccl2* were increased in response to HFD in mPGES-1^{+/+} but not in mPGES-1^{-/-} mice (Figure 4d,e). No changes in *Tnfa* or the lymphocyte marker *Cd3* expression were observed between groups (Figure 4f,g). The expression of *Adipoq* (Figure 4h) did not change with HFD but it was diminished in HFD-fed mPGES-1^{-/-} mice. We did not observe differences in inflammatory markers or adiponectin in PVAT from mice given normal diet (Figure 4d–h).

3.5 | mPGES-1 deficiency partially protects against HFD-induced structural and mechanical alterations

HFD increased aorta cross-sectional area in mPGES-1^{+/+} but not in mPGES-1^{-/-} mice (Figure 5a). Structural and mechanical properties were similar in mesenteric resistance arteries from control male mPGES-1^{+/+} and mPGES-1^{-/-} mice although mPGES-1^{-/-} mice showed greater wall stress likely due to slight, but not significant, differences in lumen diameter and wall thickness (Figure 5b–g). HFD decreased lumen diameter in arteries from both genotypes although statistical significance was only reached in knockout mice (Figure 5b). Moreover, wall thickness was higher in mPGES-1^{+/+} than mPGES-1^{-/-} mice fed with HFD (Figure 5c). This geometric adaptation in mPGES-1 knockout mice normalized circumferential wall stress that was otherwise decreased in obese wild type animals, probably to protect the vessel wall from possible changes in intraluminal pressure (Figure 5d). Strain was decreased by HFD in both genotypes (Figure 5e). Moreover, incremental distensibility was decreased and vascular stiffness was increased by HFD in mPGES-1^{+/+} but not in knockout mice (Figure 5f,g).

We then looked at vascular and PVAT fibrosis markers. We found no differences between groups in collagen and *Tgfb* expression in aorta (Figure S3A,B). HFD increased *Fn1* expression in aortic PVAT from mPGES-1^{+/+} but not in mPGES-1^{-/-} mice (Figure S3C). However, *Tgfb* and *Ctgf* gene expression remained unchanged by diet or genotype in aortic PVAT (Figure S3D,E). No differences were found in 3D elastin structure in the internal elastic lamina of mesenteric arteries between groups (Figure S3F).

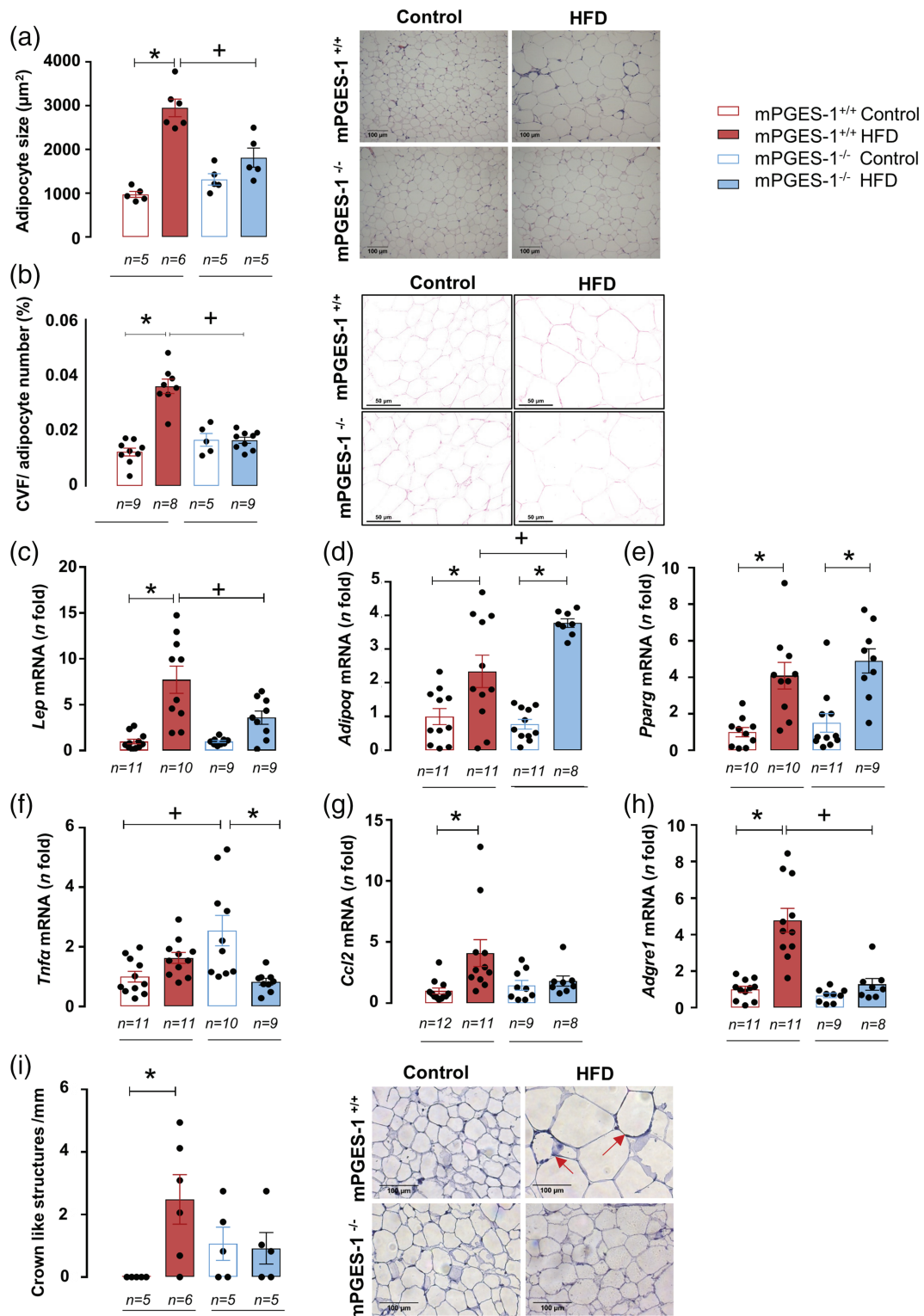
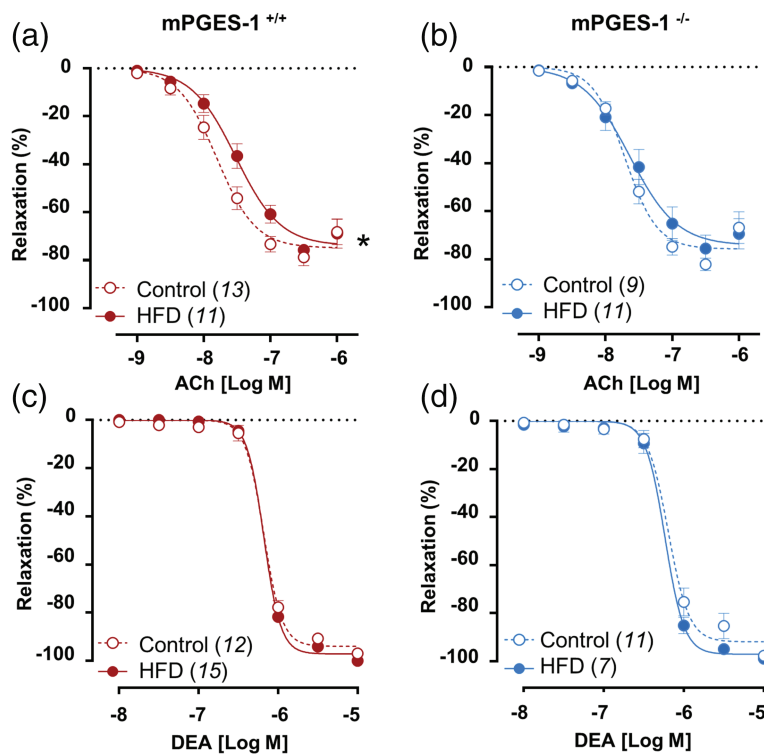


FIGURE 2 mPGES-1 deficiency prevents adiposity, fibrosis, and inflammation in abdominal adipose tissue. (a) Adipocyte size in haematoxylin–eosin-stained sections of abdominal WAT from mPGES-1^{+/+} and mPGES-1^{-/-} mice fed with normal diet (control) and high fat diet (HFD). Representative images are shown. (b) Quantification and representative images of collagen volume fraction (CVF) of Sirius red stained-WAT. mRNA levels of *Lep* (c), *Adipoq* (d), *Pparg* (e), *Tnfa* (f), *Ccl2* (g), and *Adgre1* (h) in adipose tissue from each experimental group.

(i) Quantification and representative images of crown-like structures in sections of abdominal WAT. Arrows show crown-like structures. In all bar graphs, each dot represents one mouse. Data shown are individual values with means \pm SEM. * $P < 0.05$, significantly different from control of each genotype. + $P < 0.05$, significantly different from mPGES-1^{+/+} under the same diet; one-way ANOVA or non-parametric Kruskal–Wallis test. The number of animals in each group is shown below each bar

Aorta



MRA

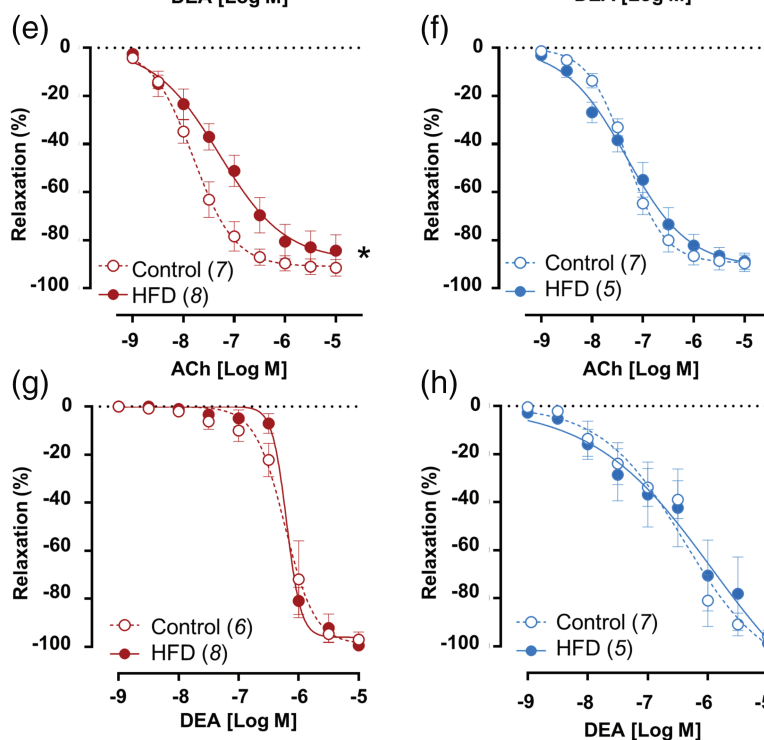


FIGURE 3 mPGES-1 deficiency protects against endothelial dysfunction induced by high fat diet (HFD) in aortic and mesenteric resistance arteries. Concentration-response curves to acetylcholine (ACh) and diethylamine NONOate (DEA-NO) of aorta (a–d) and mesenteric resistance arteries (MRA) (e–h) from mPGES-1^{+/+} and mPGES-1^{-/-} mice fed with normal diet (control) and HFD. Data represent mean \pm SEM. * $P < 0.05$, significantly different from control; two-way ANOVA. The number of animals in each group is shown in parentheses

3.6 | mPGES-1 deficiency partially protects against HFD-induced cardiac hypertrophy and fibrosis

Heart structure or extracellular matrix proteins were unaltered in male mice from both genotypes fed on normal diet (Figures 6 and 7). HFD induced cardiac hypertrophy and cardiomyocyte hypertrophy in

mPGES-1^{+/+} but not in knockout mice (Figure 6a,b). We found no significant differences in the expression of hypertrophy markers *Acta2*, *Nppa*, or α -SMA (Figure 6c–e).

No changes in gene expression of the profibrotic markers *Tgfb*, *Colla2*, or *Col3a1* were observed between groups (Figure 7a–c). However, HFD increased TGF- β protein and collagen deposition at

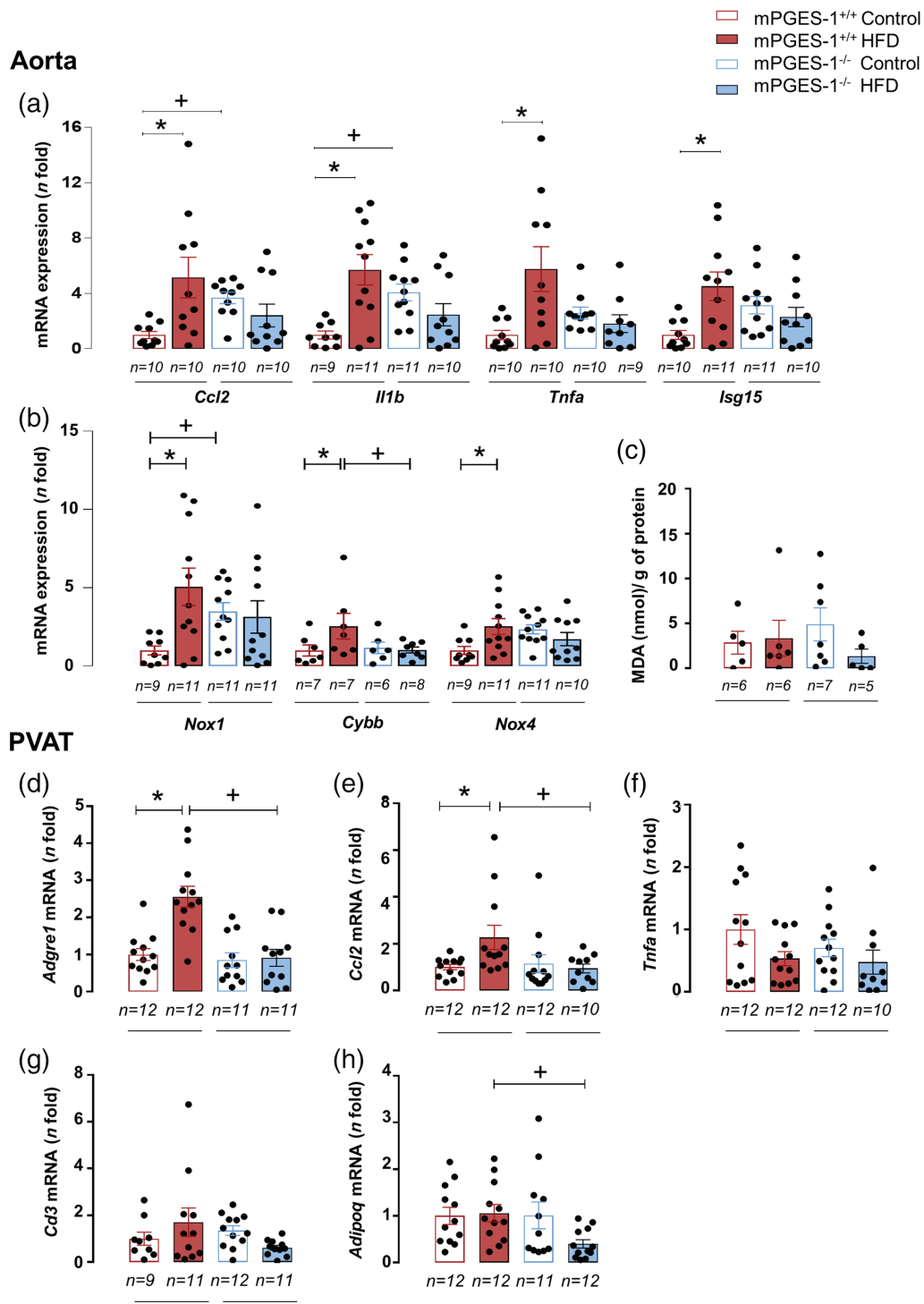


FIGURE 4 mPGES-1 deficiency protects against vascular and perivascular adipose tissue (PVAT) inflammation, induced by a high fat diet (HFD). mRNA levels of *Ccl2*, *Il1b*, *Tnfa*, and *Isg15* (a), and the NADPH oxidase subunits *Nox1*, *Cybb* (*Nox2*), and *Nox4* (b) in aorta homogenates from mPGES-1^{+/+} and mPGES-1^{-/-} mice fed with normal diet (control) and HFD. (c) Malondialdehyde (MDA) levels in aorta homogenates of each experimental group. mRNA levels of *Adgre1* (d), *Ccl2* (e), *Tnfa* (f), *Cd3* (g), and *Adipoq* (h), in PVAT homogenates from mPGES-1^{+/+} and mPGES-1^{-/-} mice fed with normal diet (control) and HFD. In all bar graphs, each dot represents one mouse. Data shown are individual values with means \pm SEM. * $P < 0.05$, significantly different from control of each genotype. + $P < 0.05$, significantly different from mPGES-1^{+/+} under the same diet; one-way ANOVA or non-parametric Kruskal–Wallis test. The number of animals in each group is shown below each bar

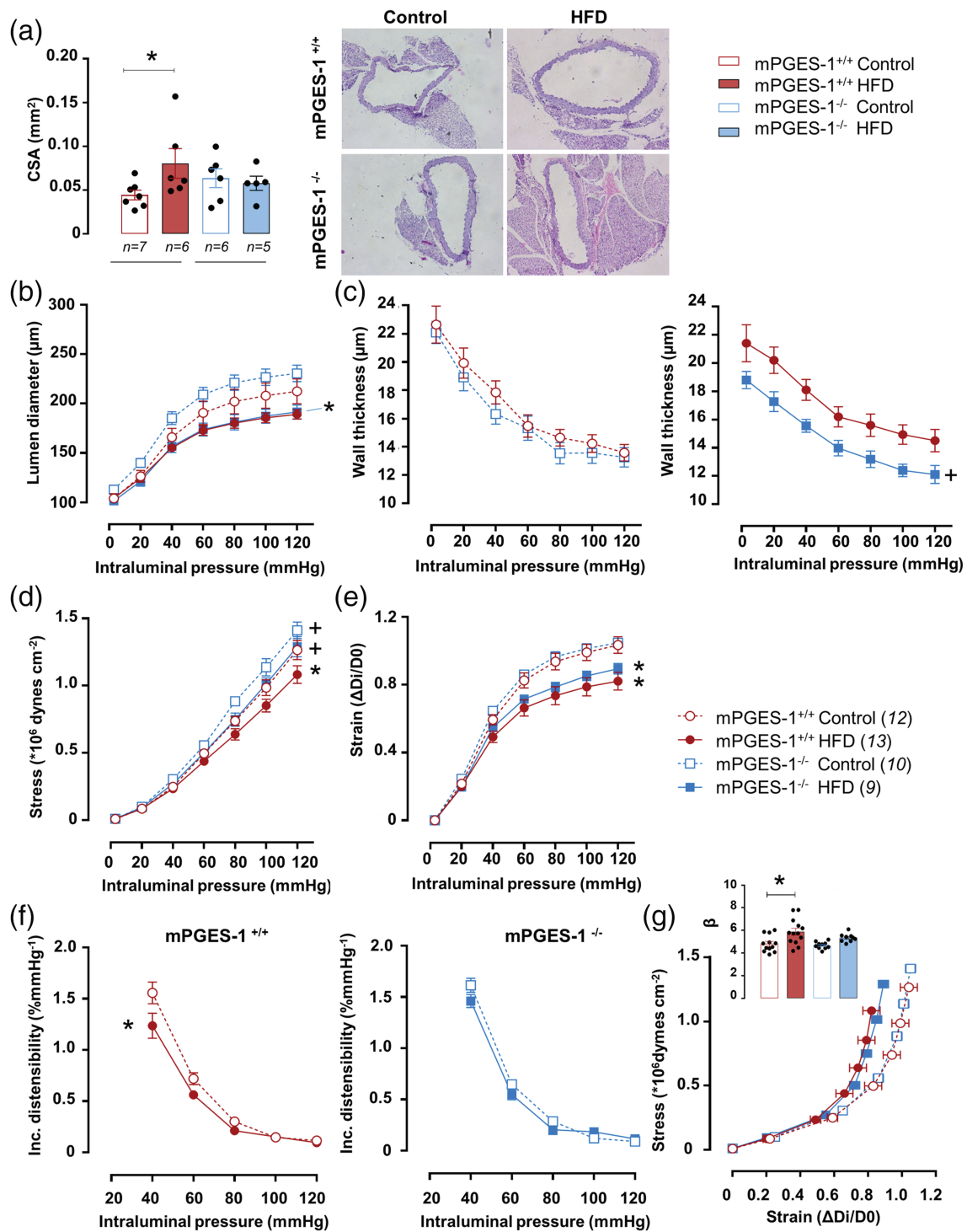


FIGURE 5 mPGES-1 deficiency partly protects against structural alterations in aorta and mesenteric resistance arteries, induced by a high fat diet (HFD). (a) Wall cross sectional area (CSA) and representative images of haematoxylin and eosin-stained aortas from mPGES-1^{+/+} and mPGES-1^{-/-} mice fed with normal diet (control) and HFD. Structural (b,c) and mechanical (d-g) parameters in mesenteric resistance arteries from each experimental group. In bar graphs, each dot represents one mouse. Data shown are means ± SEM, with individual values in (a, g inset). **P* < 0.05, significantly different from control of each genotype. +*P* < 0.05, significantly different from mPGES-1^{+/+} under the same diet; one-way (a, g inset) or two-way ANOVA or non-parametric Kruskal-Wallis test (b-f). The number of animals in each group is shown in parentheses or below each bar

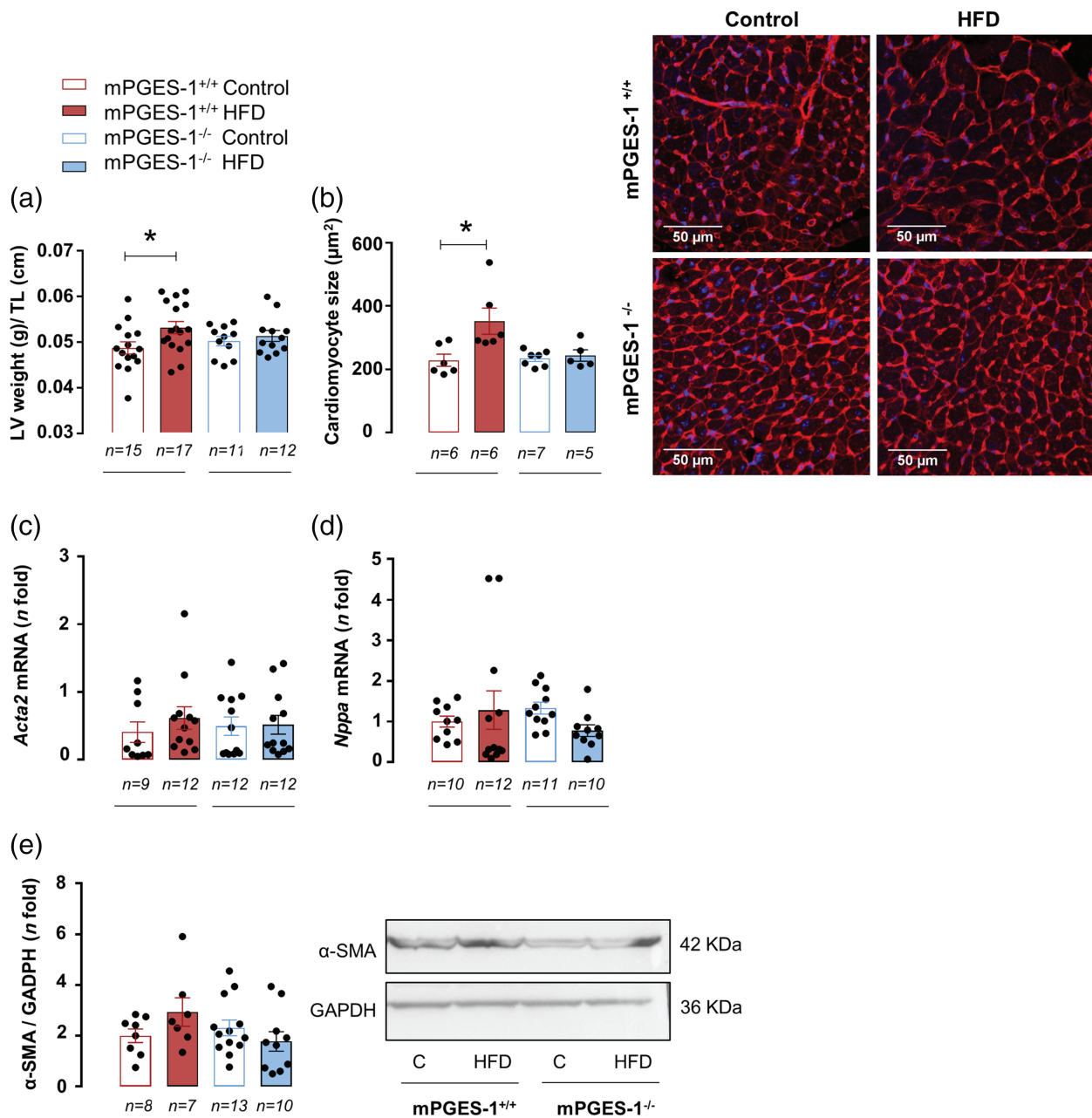


FIGURE 6 mPGES-1 deficiency protects against cardiac hypertrophy, induced by a high fat diet (HFD). (a) Left ventricle (LV) weight normalized to tibia length (TL) and (b) mean cardiomyocyte size and representative images of WGA-stained cardiomyocytes from mPGES-1^{+/+} and mPGES-1^{-/-} mice fed with normal (control) and HFD. (c) *Acta-2* and (d) *Nppa* mRNA expression in cardiac lysates. (e) Protein expression of α-SMA in cardiac homogenates from each experimental group. Representative blots are also shown. In all bar graphs, data shown are individual values with means ± SEM. **P* < 0.05, significantly different from control; one-way ANOVA or non-parametric Kruskal–Wallis test. The number of animals in each group is shown below each bar

the heart in wild-type mice but not in mPGES-1 deficient mice (Figure 7d,e). Moreover, there was a positive correlation between cardiac fibrosis and hypertrophy (Figure 7f). Also, *Colla2* but not *Col3a1* positively correlated with *Tgfb* expression (Figure 7g,h). We then looked at cardiac oxidative stress and inflammatory markers and found no significant differences between groups neither in gene expression nor in MDA levels (Figure S4).

3.7 | mPGES-1 deficiency also protects against some of the metabolic and cardiovascular alterations associated with obesity in female mice

No differences in body weight gain or glucose levels were observed in female mPGES-1^{+/+} and mPGES-1^{-/-} fed on normal diet (Figure S5). However, similarly to male mice, HFD-induced weight gain was

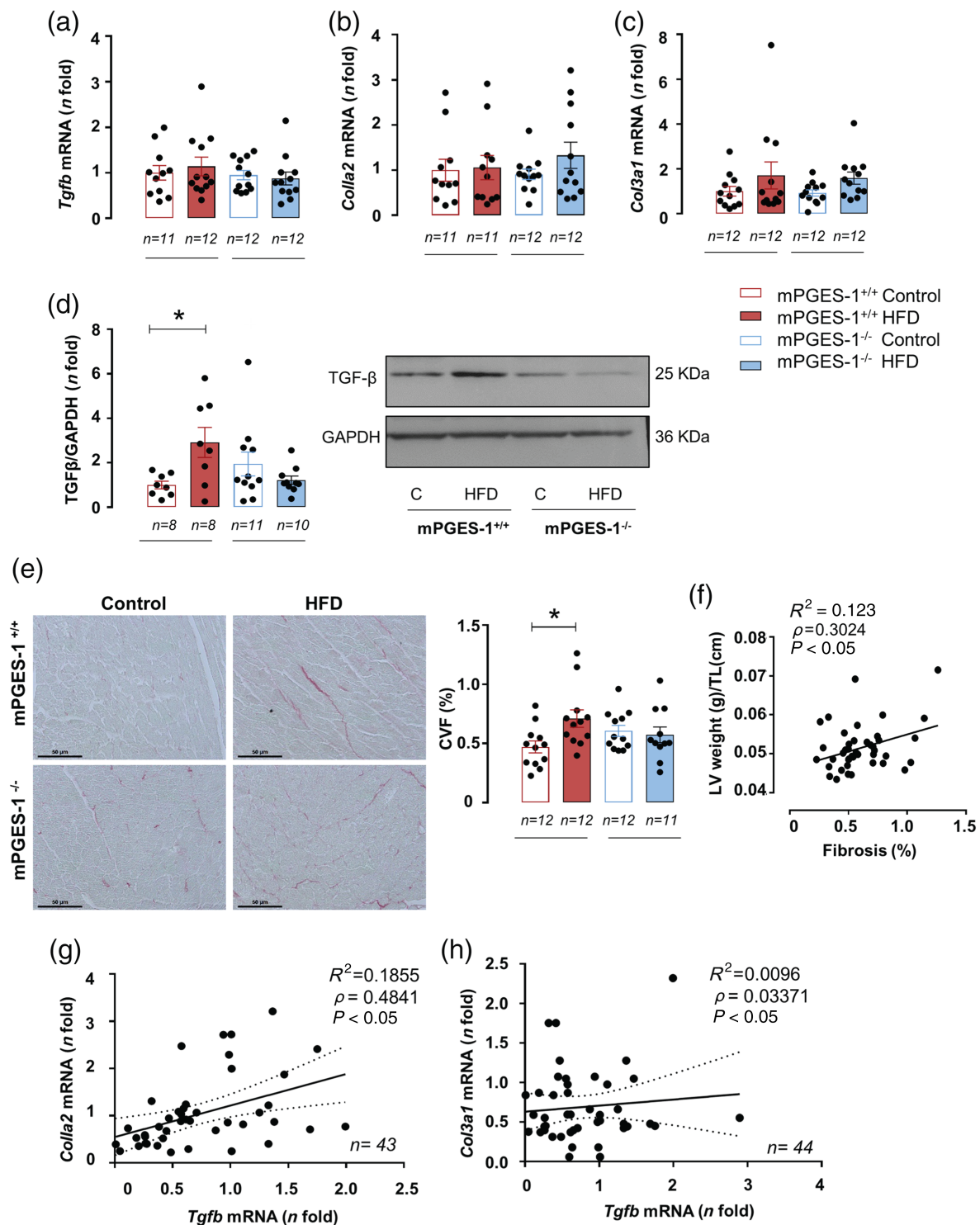


FIGURE 7 mPGES-1 deficiency partly protects against cardiac fibrosis induced by a high fat diet (HFD). mRNA levels of *Tgfb* (a), *Col1a2* (b), and *Col3a1* (c) in hearts from mPGES-1^{+/+} and mPGES-1^{-/-} mice fed with normal (control) and HFD. (d) Protein expression of TGF- β in cardiac homogenates from each experimental group. Representative blots are also shown. (e) Representative images and quantification of collagen volume fraction (CVF) of Sirius red stained hearts sections from all groups. (f) Correlation by Spearman *t*-test of the percentage of cardiac hypertrophy, measured as the ratio of left ventricular (LV) weight to tibia length (TL), with fibrosis, measured as CVF; correlations of the expression of *Col1a2* (g) and *Col3a1* (h) with expression of *Tgfb*. The data shown in (f) and (g) were significantly ($P < 0.05$) correlated. Data shown in bar graphs are individual values with means \pm SEM. * $P < 0.05$, significantly different from control; one-way ANOVA or non-parametric Kruskal-Wallis test. The number of animals in each group is shown below each bar

significantly higher in female mPGES-1^{+/+} mice than in mPGES-1^{-/-} animals (Figure S5A) although this difference seems to be less marked than in males (Figure 1a). Perirenal fat weight was significantly increased by HFD only in wild type mice (Table S4). Moreover, WAT weight and adiposity index were smaller in HFD-fed mPGES-1^{-/-} mice, compared with mPGES-1^{+/+} mice (Table S4).

Basal glucose levels and GTT were comparably increased by HFD in both genotypes (Figure S5B–D). No differences in insulin sensitivity were observed between genotypes (Figure S5E,F).

Regarding cardiovascular alterations, we found no differences between groups in SBP (Table S5). In aorta from females, HFD did not modify endothelium-dependent relaxation to acetylcholine or insulin in any of the genotypes (Figures S6A,B and S7A,B), indicating some vascular protection by gender. However, HFD induced endothelial dysfunction in mesenteric resistance arteries from mPGES-1^{+/+} but not in mPGES-1^{-/-} mice (Figure S6E,F). No differences in vasodilator responses to DEA-NO were observed between the experimental groups neither in aorta (Figure S6C,D) nor in mesenteric arteries (Figure S6G,H). HFD-induced heart hypertrophy was similar in mPGES-1^{+/+} and mPGES-1^{-/-} mice (Figure S7C).

3.8 | mPGES-1 expression in human abdominal fat correlates with vascular remodelling, vascular stiffness, and SPB

Given the beneficial effects of mPGES-1 deletion in the animal model, we evaluated a possible relationship between expression of mRNA for mPGES-1 in abdominal adipose tissue and vascular damage in humans. *PTGES* expression did not correlate with BMI (Figure 8a) but it positively correlated with SBP (Figure 8b), IMT (Figure 8c), and vascular stiffness measured as PWV (Figure 8d).

3.9 | mPGES-1 expression in PVAT of aortic abdominal aneurysm patients correlates with inflammation

Because mPGES-1 deletion reduced obesity-induced inflammatory cells infiltration in PVAT (Figure 4), we used human aortic PVAT to analyse a potential correlation between *PTGES* expression and that of immune cell markers in this specific adipose tissue depot. As shown in Figure 8e, expression of *PTGES* in PVAT did not correlate with body mass index. However, *PTGES* expression positively correlated with the macrophage marker *CD68* (Figure 8f), the T lymphocytes markers (*CD3G*, *CD4*, and *CD8A*) (Figure 8g–i) and with *LEP* (Figure 8j).

4 | DISCUSSION

Selective mPGES-1 inhibitors that specifically constrain PGE₂ synthesis without affecting synthesis of the protective PGI₂ are currently under development to circumvent the cardiovascular hazards induced

by COX inhibitors while producing strong anti-inflammatory effects (Bergqvist et al., 2020). Thus, there is an urgent need to understand the role of mPGES-1 in the cardiovascular system in the context of highly prevalent clinical conditions such as obesity. Our study demonstrates that mPGES-1 deletion protects from the metabolic and cardiovascular alterations associated with obesity by mechanisms likely to be related to a decrease in inflammatory mediators.

We observed that mPGES-1^{-/-} mice developed less gain weight and had smaller adipocytes in response to HFD than wild type animals, which agrees with a recent study performed in mPGES-1 knockout mice on DBA genetic background (Pierre et al., 2018). Reasons for this adipose tissue phenotype in HFD-mPGES-1^{-/-} mice are likely to include an increase in energy expenditure without changes in browning process (Pierre et al., 2018). In addition, PGE₂ seems to have anti-lipolytic functions whereas PGI₂ stimulates lipolysis (Chatzipanteli et al., 1992), and mPGES-1 deficient mice have increased urinary, macrophage, adipose tissue and vascular PGI₂ levels in different settings including obesity (Avenidaño et al., 2018; Cheng et al., 2006; Sasaki et al., 2021; Wang et al., 2006, 2008). Of note, the smaller HFD-induced weight gain observed in mPGES-1^{-/-} mice was associated with a better metabolic profile, as shown by the improved glucose tolerance and insulin sensitivity, and lipid levels. Accordingly, inhibition of the COX-2 enzyme in humans (González-Ortiz et al., 2005) and in animal models (Hsieh et al., 2010), in the context of obesity, was associated with a better metabolic status. However, Pierre et al. (2018) found similar basal levels of glucose in mPGES-1^{+/+} and mPGES-1^{-/-}, although a complete characterization was not performed. Mechanisms responsible for insulin resistance in obesity include adipose tissue augmented inflammatory status characterized by macrophage infiltration and enhanced TNF-α production, and dysregulation of adiponectin and leptin levels (Petersen & Shulman, 2018; Stern et al., 2016). Indeed, insulin resistance in obese individuals is associated with adipose tissue dysfunction, inflammation, and an imbalance of circulating adipokines independently of total body fat mass (Stern et al., 2016). Additionally, a rigid extracellular matrix may exert shear stress on expanding adipocytes, leading to adipocyte cell death and consequent inflammation (Datta et al., 2018). Accordingly, we observed that HFD mPGES-1^{-/-} mice showed increased levels of *Adipoq* and decreased *Lep* levels and collagen deposition and showed protection against inflammatory features that might have contributed to a better metabolic profile.

In obesity, adipose tissue dysfunction leads to an inflammatory state that could trigger cardiovascular alterations (Fuster et al., 2016). Thus, insulin resistance, PVAT inflammation and NADPH oxidase overexpression with the subsequent reduction in NO availability associated with obesity, trigger endothelial dysfunction (Engin, 2017; Kobayasi et al., 2010). Production of prostanoids including TXA₂, 6-keto-PGF_{1α} and PGE₂ was increased in aorta from a rat model of obesity, induced by monosodium glutamate administration (Majewski et al., 2018). We did not observe changes in cardiac, vascular, or PVAT mPGES-1 mRNA expression in response to obesity and PGE₂ levels were not modified either by diet or genotype in aorta or heart, suggesting that most of the detected PGE₂ derives from the

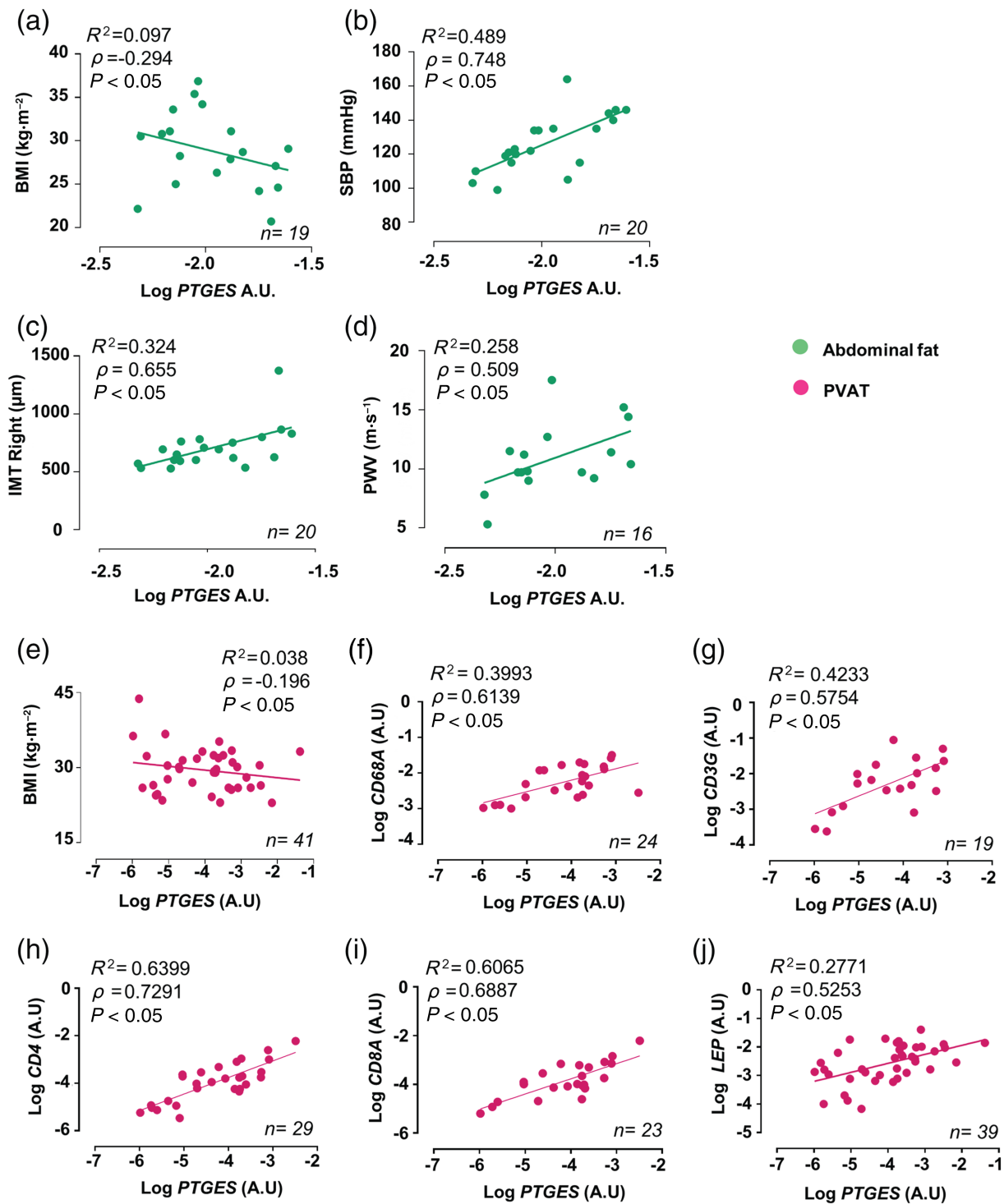


FIGURE 8 mPGES-1 expression in human abdominal adipose tissue or perivascular adipose tissue (PVAT) correlates with parameters of vascular damage and inflammation. Correlation between mRNA levels of *PTGES* in human abdominal adipose tissue and body mass index (BMI) (a), systolic blood pressure (SBP) (b), intima-media thickness (IMT) (c), and pulse wave velocity (PWV) (d). Correlation between mRNA levels of *PTGES* in PVAT of patients with aortic aneurysms and body mass index (BMI) (e), *CD68* (f), *CD3* (g), *CD4* (h), *CD8* (i), and *LEP* (j). Each dot represents one patient. Correlations were calculated with Spearman t -test and were significant ($P < 0.05$) for all data sets shown except for those with BMI, shown in (a) and (e). The number of patients is shown in each graph

constitutive PGE₂ synthases. However, we demonstrate for the first time, that mPGES-1 has a key role in the vascular alterations observed in obesity. Thus, the HFD-induced endothelial dysfunction of conductance and resistance arteries and the vascular insulin resistance observed in wild-type mice, was completely prevented by mPGES-1 knockdown. Moreover, mPGES-1 deletion partly prevented vascular remodelling and mechanical alterations induced by HFD, although the specific proteins involved need to be further studied. The role of mPGES-1 in vascular damage has already been explored in the context of other pathologies, with divergent results. Specifically, in mPGES-1 deficient mice, we recently observed vascular protection against hypertension-induced endothelial dysfunction, hypercontractility and structural alterations (Avenidaño et al., 2018), and other authors found less aneurysm formation (Wang et al., 2008), atherosclerosis development (Wang et al., 2006) and neointima thickening in response to injury (Wang et al., 2011). However, other studies have suggested a protective role of mPGES-1 against myocardial ischaemia reperfusion injury by vascular mechanisms (Zhu et al., 2019). More importantly, we found positive correlations between adipose tissue mPGES-1 and clinical parameters of vascular damage, that is, IMT and PWV in the absence of correlation with BMI, suggesting that the relationship between adipose tissue mPGES-1 and vascular damage in humans is not merely a consequence of altered body weight. Indeed, HFD tended to decrease the expression of *Ptges* mRNA in mice WAT and Sasaki et al. (2021) found no changes in PGE₂ levels in WAT between wild-type and mPGES-1^{-/-} mice fed on a HFD. Our data extend previous observations showing a positive correlation between peripheral blood mononuclear cells (PBMCs), mPGES-1 and BMI in humans (Avenidaño et al., 2018). Furthermore, we reported that mPGES-1 expressed in PBMCs was strongly associated with blood pressure and vascular remodelling (Avenidaño et al., 2018). In agreement, mice lacking mPGES-1 conditionally in myeloid cells, when crossed into hyperlipidaemic LDLR-deficient animals, showed reduced atherogenesis (Chen et al., 2014). Altogether, these results suggest a role for mPGES-1, likely from a range of different cell types including vascular cells, immune cells, and adipocytes, in the vascular damage associated with obesity. Moreover, although our preclinical model of obesity did not show increased blood pressure, we observed a positive correlation of adipose tissue mPGES-1 and SBP in humans, a clinical condition frequently observed in human obesity.

Underlying mechanisms responsible for the beneficial effects of mPGES-1 deletion in obesity-induced vascular damage are likely to include both vascular mechanisms and improved crosstalk with surrounding PVAT. In this sense, it is accepted that PVAT might have a role in vascular damage in obesity and other pathologies such as AAA because of the infiltration of inflammatory macrophages and T cells (Fernández-Alfonso et al., 2017). In mPGES-1^{-/-} mice, HFD did not increase aortic gene expression of inflammatory cytokines involved in endothelial dysfunction or vascular remodelling including *Ccl2*, *I11b*, *Tnfa*, or *Isg15*, and NADPH oxidase isoforms (*Nox1/2/4*), as opposed to wild type mice. In agreement, mPGES-1 deletion reduced vascular oxidative stress in both hypertensive and aneurysmal models (Avenidaño et al., 2018; Wang et al., 2008). Moreover, PVAT from

mPGES-1^{-/-} mice had less infiltration of macrophages that would eventually result in lower production of inflammatory cytokines. Importantly, this might have clinical implications as we observed positive correlations between mPGES-1 expression and macrophages and T cells infiltration in aortic PVAT from patients with AAA. Increased synthesis of the vasculoprotective PGI₂ in mPGES-1 deficient mice might also contribute to the beneficial effects of mPGES-1 deletion in obesity, as shown previously in hypertension and other vascular pathologies (Avenidaño et al., 2018; Wang et al. 2006 and 2008), and this warrants further investigation. In this sense, in healthy humans, the pharmacological inhibitor of mPGES-1, LY3023703 increased the levels of urinary PGI₂ compared with placebo (Jin et al., 2016) and the mPGES-1 inhibitor **C3 compound** increased PGI₂ release in internal mammary artery and saphenous vein, associated with decreased vascular tone (Ozen et al., 2017). Finally, a contribution of the better metabolic profile and greater weight loss observed in mPGES-1 knockout mice cannot be fully excluded.

We found that cardiac hypertrophy positively correlated with the percentage of fibrosis, which is known to impair cardiac function (Martínez-Martínez et al., 2015). We also provided novel evidence demonstrating that mPGES-1 deletion prevents obesity-induced cardiac and cardiomyocytes hypertrophy and fibrosis and expression of some profibrotic markers suggesting some degree of cardiac protection. A limitation of our study is that we have not performed a full characterization of the cardiac damage at the functional and molecular level. Indeed, to our surprise, we did not detect significant changes in inflammatory mediators in our cardiac samples. The effects of mPGES-1 deletion in cardiac damage have provided controversial results depending on the experimental model. In mice, the lack of mPGES-1 prevents the acute post-myocardial infarction death (Wu et al., 2009) or fibrosis induced by agonists of β- adrenoceptors (Ji et al., 2020). However, mPGES-1 deletion impairs left ventricular contractile function after acute myocardial infarction (Degousee et al., 2008) or after chronic **angiotensin II** infusion (Harding et al., 2011) and impairs cardiac microvascular perfusion in a myocardial ischaemia reperfusion model (Zhu et al., 2019). Although further dedicated studies are needed, the different contribution of haemodynamic, metabolic, or inflammatory mechanisms in models of hypertension, myocardial infarction, and obesity could underlie these discrepancies.

Another important result is that some of the beneficial effects induced by mPGES-1 deletion in males were also reproduced in females. There is a historical paucity of studies performed in females probably due to the metabolic and cardiovascular protection elicited by oestrogens on insulin sensitivity, glucose tolerance, body weight gain, and adiposity in models of HFD-induced obesity (Handgraaf et al., 2013; Riant et al., 2009). In fact, we found that, given the same HFD, female mice gained similar weight to males but showed no endothelial dysfunction or vascular insulin resistance of the aorta, although in resistance arteries, endothelial function was similarly impaired. As in males, the absence of mPGES-1 in females partly protected against HFD-induced body weight gain, adiposity, and improved resistance arteries endothelial dysfunction induced by HFD.

However, a reduced weight gain seems to be more pronounced in male mPGES-1^{-/-} than in female knockout mice and mPGES-1 deletion did not improve the insulin sensitivity, glucose tolerance or gross cardiac hypertrophy induced by HFD.

In conclusion, we demonstrate that in male mice, mPGES-1 deletion confers protection against body weight gain, adipose tissue enlargement and the glycaemic and lipid alterations induced by HFD. Moreover, we demonstrate for the first time that the absence of mPGES-1 protects against adipose tissue and cardiac hypertrophy and fibrosis, and endothelial dysfunction and vascular remodelling induced by obesity. Underlying mechanisms are likely to include decreased inflammation in adipose tissue depots and the vasculature. Moreover, some of the beneficial effects of mPGES-1 deletion were also reproduced in female mice. In human tissue samples, mPGES-1 expression in abdominal or perivascular adipose tissue correlated with parameters of vascular remodelling, stiffness, and inflammation. Thus, selective inhibitors of mPGES-1 might be a useful therapeutic tool against the metabolic and cardiovascular alterations induced by obesity.

ACKNOWLEDGEMENTS

This work was supported by the Ministerio de Ciencia e Innovación and Fondo Europeo de Desarrollo Regional (FEDER)/FSE (SAF2016-80305P), Instituto de Salud Carlos III (ISCIII; FIS PI18/0257); Comunidad de Madrid (CM) (B2017/BMD-3676 AORTASANA) FEDER-a way to build Europe. MGA was supported by a FPI-UAM fellowship and RRD by a Juan de la Cierva contract (IJCI-2017-31399). The authors thank Victor Gutierrez his help with some experiments.

AUTHOR CONTRIBUTIONS

CB-M and RR-D wrote the manuscript and researched data. LMB, RM-C, EM-M, MG-A, and CR researched data. AM-B reviewed/edited and wrote the manuscript. VC, MS, and JM-G contributed to discussion and reviewed/edited manuscript. All authors approved the manuscript.

CONFLICT OF INTEREST

The authors have declared that no conflict of interest exists.

DECLARATION OF TRANSPARENCY AND SCIENTIFIC RIGOUR

This Declaration acknowledges that this paper adheres to the principles for transparent reporting and scientific rigour of preclinical research as stated in the *BJP* guidelines for [Design and Analysis](#), [Immunoblotting and Immunochemistry](#), and [Animal Experimentation](#), and as recommended by funding agencies, publishers and other organizations engaged with supporting research.

DATA AVAILABILITY STATEMENT

Constanza Ballesteros-Martínez, Raquel Rodrigues-Diez, and Ana M. Briones had full access to all the data in the study and take responsibility for the integrity of the data and the accuracy of the data

analysis. The data supporting the findings of this study are available from the corresponding authors upon reasonable request. Some data may not be made available because of privacy or ethical restrictions.

ORCID

Raquel Rodrigues-Diez  <https://orcid.org/0000-0002-6348-1505>

Ana M. Briones  <https://orcid.org/0000-0001-8218-5579>

REFERENCES

- Alexander, S. P., Christopoulos, A., Davenport, A. P., Kelly, E., Mathie, A., Peters, J. A., Veale, E. L., Armstrong, J. F., Faccenda, E., Harding, S. D., Pawson, A. J., Southan, C., Davies, J. A., Abbracchio, M. P., Alexander, W., Al-hosaini, K., Bäck, M., Barnes, N. M., Bathgate, R., ... Ye, R. D. (2021). The Concise Guide to PHARMACOLOGY 2021/22: G protein-coupled receptors. *British Journal of Pharmacology*, 178(S1), S27–S156. <https://doi.org/10.1111/bph.15538>
- Alexander, S. P., Cidlowski, J. A., Kelly, E., Mathie, A., Peters, J. A., Veale, E. L., Armstrong, J. F., Faccenda, E., Harding, S. D., Pawson, A. J., Southan, C., Davies, J. A., Coons, L., Fuller, P. J., Korach, K. S., & Young, M. J. (2021). The Concise Guide to PHARMACOLOGY 2021/22: Nuclear hormone receptors. *British Journal of Pharmacology*, 178(S1), S246–S263. <https://doi.org/10.1111/bph.15540>
- Alexander, S. P., Fabbro, D., Kelly, E., Mathie, A., Peters, J. A., Veale, E. L., Armstrong, J. F., Faccenda, E., Harding, S. D., Pawson, A. J., Southan, C., Davies, J. A., Boison, D., Burns, K. E., Dessauer, C., Gertsch, J., Helsby, N. A., Izzo, A. A., Koesling, D., ... Wong, S. S. (2021). The Concise Guide to PHARMACOLOGY 2021/22: Enzymes. *British Journal of Pharmacology*, 178(S1), S313–S411. <https://doi.org/10.1111/bph.15542>
- Alexander, S. P., Kelly, E., Mathie, A., Peters, J. A., Veale, E. L., Armstrong, J. F., Faccenda, E., Harding, S. D., Pawson, A. J., Southan, C., Buneman, O. P., Cidlowski, J. A., Christopoulos, A., Davenport, A. P., Fabbro, D., Spedding, M., Striessnig, J., Davies, J. A., Ahlers-Dannen, K. E., ... Zolghadri, Y. (2021). The Concise Guide to PHARMACOLOGY 2021/22: Other Protein Targets. *British Journal of Pharmacology*, 178(S1), S1–S26. <https://doi.org/10.1111/bph.15537>
- Avendaño, M. S., García-Redondo, A. B., Zalba, G., González-Amor, M., Aguado, A., Martínez-Revelles, S., Beltrán, L. M., Camacho, M., Cachofeiro, V., Alonso, M. J., Salices, M., & Briones, A. M. (2018). mPGES-1 (microsomal prostaglandin E synthase-1) mediates vascular dysfunction in hypertension through oxidative stress. *Hypertension (Dallas, Tex: 1979)*, 72(2), 492–502. <https://doi.org/10.1161/HYPERTENSIONAHA.118.10833>
- Bergqvist, F., Morgenstern, R., & Jakobsson, P. J. (2020). A review on mPGES-1 inhibitors: From preclinical studies to clinical applications. *Prostaglandins & Other Lipid Mediators*, 147, 106383. <https://doi.org/10.1016/j.prostaglandins.2019.106383>
- Briones, A. M., Aras-López, R., Alonso, M. J., & Salices, M. (2014). Small artery remodeling in obesity and insulin resistance. *Current Vascular Pharmacology*, 12(3), 427–437. <https://doi.org/10.2174/157016112666140423221319>
- Buettner, R., Schölmerich, J., & Bollheimer, L. C. (2007). High-fat diets: Modeling the metabolic disorders of human obesity in rodents. *Obesity (Silver Spring, Md.)*, 15(4), 798–808. <https://doi.org/10.1038/oby.2007.608>
- Chan, P. C., Hsiao, F. C., Chang, H. M., Wabitsch, M., & Hsieh, P. S. (2016). Importance of adipocyte cyclooxygenase-2 and prostaglandin E2-prostaglandin E receptor 3 signaling in the development of obesity-induced adipose tissue inflammation and insulin resistance. *FASEB Journal: Official Publication of the Federation of American*

- Societies for Experimental Biology*, 30(6), 2282–2297. <https://doi.org/10.1096/fj.201500127>
- Chatzipanteli, K., Rudolph, S., & Axelrod, L. (1992). Coordinate control of lipolysis by prostaglandin E2 and prostacyclin in rat adipose tissue. *Diabetes*, 41(8), 927–935. <https://doi.org/10.2337/diab.41.8.927>
- Chen, L., Yang, G., Monslow, J., Todd, L., Cormode, D. P., Tang, J., Grant, G. R., DeLong, J. H., Tang, S. Y., Lawson, J. A., Pure, E., & Fitzgerald, G. A. (2014). Myeloid cell microsomal prostaglandin E synthase-1 fosters atherogenesis in mice. *Proceedings of the National Academy of Sciences of the United States of America*, 111(18), 6828–6833. <https://doi.org/10.1073/pnas.1401797111>
- Cheng, Y., Wang, M., Yu, Y., Lawson, J., Funk, C. D., & Fitzgerald, G. A. (2006). Cyclooxygenases, microsomal prostaglandin E synthase-1, and cardiovascular function. *The Journal of Clinical Investigation*, 116(5), 1391–1399. <https://doi.org/10.1172/JCI27540>
- Curtis, M. J., Alexander, S., Cirino, G., Docherty, J. R., George, C. H., Giembycz, M. A., Hoyer, D., Insel, P. A., Izzo, A. A., Ji, Y., MacEwan, D. J., Sobey, C. G., Stanford, S. C., Teixeira, M. M., Wonnacott, S., & Ahluwalia, A. (2018). Experimental design and analysis and their reporting II: Updated and simplified guidance for authors and peer reviewers. *British Journal of Pharmacology*, 175(7), 987–993.
- Dan, H. J., Wang, Y., Zeng, M. X., Luan, Y. Y., & Hu, B. (2011). Evaluation of intima-media thickness and vascular elasticity of the common carotid artery in patients with isolated systolic hypertension using ultrasound radiofrequency-data technology. *Clinical Physiology and Functional Imaging*, 31(4), 315–319.
- Datta, R., Podolsky, M. J., & Atabai, K. (2018). Fat fibrosis: Friend or foe? *The Journal of Clinical Investigation Insight*, 3(19), e122289. <https://doi.org/10.1172/jci.insight.122289>
- Degousee, N., Fazel, S., Angoulvant, D., Stefanski, E., Pawelzik, S. C., Korotkova, M., Arab, S., Liu, P., Lindsay, T. F., Zhuo, S., Butany, J., Li, R.-K., Audoly, L., Schmidt, R., Angioni, C., Geisslinger, G., Jakobsson, P.-J., & Rubin, B. B. (2008). Microsomal prostaglandin E2 synthase-1 deletion leads to adverse left ventricular remodeling after myocardial infarction. *Circulation*, 117(13), 1701–1710. <https://doi.org/10.1161/CIRCULATIONAHA.107.749739>
- Engin, A. (2017). Endothelial dysfunction in obesity. *Advances in Experimental Medicine and Biology*, 960, 345–379. https://doi.org/10.1007/978-3-319-48382-5_15
- Even, S. E., Dulak-Lis, M. G., Touyz, R. M., & Cat, A. N. D. (2014). Crosstalk between adipose tissue and blood vessels in cardiometabolic syndrome: Implication of steroid hormone receptors (MR/GR). *Hormone Molecular Biology and Clinical Investigation*, 19(2), 89–101. <https://doi.org/10.1515/hmbci-2014-0013>
- Fain, J. N., Ballou, L. R., & Bahouth, S. W. (2001). Obesity is induced in mice heterozygous for cyclooxygenase-2. *Prostaglandins & Other Lipid Mediators*, 65(4), 199–209. [https://doi.org/10.1016/S0090-6980\(01\)00136-8](https://doi.org/10.1016/S0090-6980(01)00136-8)
- Fain, J. N., Kanu, A., Bahouth, S. W., Cowan, G. S. Jr., Hiler, M. L., & Leffler, C. W. (2002). Comparison of PGE2, prostacyclin and leptin release by human adipocytes versus explants of adipose tissue in primary culture. *Prostaglandins, Leukotrienes, and Essential Fatty Acids*, 67(6), 467–473. <https://doi.org/10.1054/plef.2002.0430>
- Fernández-Alfonso, M. S., Somoza, B., Tsvetkov, D., Kuczanski, A., Dashwood, M., & Gil-Ortega, M. (2017). Role of perivascular adipose tissue in health and disease. *Comprehensive Physiology*, 8(1), 23–59. <https://doi.org/10.1002/cphy.c170004>
- Fuster, J. J., Ouchi, N., Gokce, N., & Walsh, K. (2016). Obesity-induced changes in adipose tissue microenvironment and their impact on cardiovascular disease. *Circulation Research*, 118(11), 1786–1807. <https://doi.org/10.1161/CIRCRESAHA.115.306885>
- García-Alonso, V., & Clària, J. (2014). Prostaglandin E2 signals white-to-brown adipogenic differentiation. *Adipocytes*, 3(4), 290–296. <https://doi.org/10.4161/adip.29993>
- García-Alonso, V., Titos, E., Alcaraz-Quiles, J., Rius, B., Lopategi, A., López-Vicario, C., Jakobsson, P.-J., Delgado, S., Lozano, J., & Clària, J. (2016). Prostaglandin E2 exerts multiple regulatory actions on human obese adipose tissue remodeling, inflammation, adaptive thermogenesis and lipolysis. *PLoS ONE*, 11(4), e0153751. <https://doi.org/10.1371/journal.pone.0153751>
- Ghoshal, S., Trivedi, D. B., Graf, G. A., & Loftin, C. D. (2011). Cyclooxygenase-2 deficiency attenuates adipose tissue differentiation and inflammation in mice. *The Journal of Biological Chemistry*, 286(1), 889–898. <https://doi.org/10.1074/jbc.M110.139139>
- González-Ortiz, M., Pascoe-González, S., Kam-Ramos, A. M., & Hernández-Salazar, E. (2005). Effect of celecoxib, a cyclooxygenase-2-specific inhibitor, on insulin sensitivity, C-reactive protein, homocysteine, and metabolic profile in overweight or obese subjects. *Metabolic Syndrome and Related Disorders*, 3(2), 95–101. <https://doi.org/10.1089/met.2005.3.95>
- Handgraaf, S., Riant, E., Fabre, A., Waget, A., Burcelin, R., Lière, P., Krust, A., Chambon, P., Arnal, J.-F., & Gourdy, P. (2013). Prevention of obesity and insulin resistance by estrogens requires ER α activation function-2 (ER α AF-2), whereas ER α AF-1 is dispensable. *Diabetes*, 62(12), 4098–4108. <https://doi.org/10.2337/db13-0282>
- Harding, P., Yang, X. P., He, Q., & Lapointe, M. C. (2011). Lack of microsomal prostaglandin E synthase-1 reduces cardiac function following angiotensin II infusion. *American Journal of Physiology. Heart and Circulatory Physiology*, 300(3), H1053–H1061. <https://doi.org/10.1152/ajpheart.00772.2010>
- Hétu, P. O., & Riendeau, D. (2007). Down-regulation of microsomal prostaglandin E2 synthase-1 in adipose tissue by high-fat feeding. *Obesity (Silver Spring, Md.)*, 15(1), 60–68. <https://doi.org/10.1038/oby.2007.514>
- Hsieh, P. S., Lu, K. C., Chiang, C. F., & Chen, C. H. (2010). Suppressive effect of COX2 inhibitor on the progression of adipose inflammation in high-fat-induced obese rats. *European Journal of Clinical Investigation*, 40(2), 164–171. <https://doi.org/10.1111/j.1365-2362.2009.02239.x>
- Jaworski, K., Ahmadian, M., Duncan, R. E., Sarkadi-Nagy, E., Varady, K. A., Hellerstein, M. K., Lee, H.-Y., Samuel, V. T., Shulman, G. I., Kim, K.-H., de Val, S., Kang, C., & Sul, H. S. (2009). AdPLA ablation increases lipolysis and prevents obesity induced by high-fat feeding or leptin deficiency. *Nature Medicine*, 15(2), 159–168. <https://doi.org/10.1038/nm.1904>
- Ji, S., Guo, R., Wang, J., Qian, L., Liu, M., Xu, H., Zhang, J., Guan, Y., Yang, G., & Chen, L. (2020). Microsomal prostaglandin E₂ synthase-1 deletion attenuates isoproterenol-induced myocardial fibrosis in mice. *The Journal of Pharmacology and Experimental Therapeutics*, 375(1), 40–48. <https://doi.org/10.1124/jpet.120.000023>
- Jin, Y., Smith, C. L., Hu, L., Campanale, K. M., Stoltz, R., Huffman, L. G., McNearney, T. A., Yang, X. Y., Ackermann, B. L., Dean, R., Regev, A., & Landschulz, W. (2016). Pharmacodynamic comparison of LY3023703, a novel microsomal prostaglandin e synthase 1 inhibitor, with celecoxib. *Clinical Pharmacology and Therapeutics*, 99(3), 274–284. <https://doi.org/10.1002/cpt.260>
- Kobayashi, R., Akamine, E. H., Davel, A. P., Rodrigues, M. A., Carvalho, C. R., & Rossoni, L. V. (2010). Oxidative stress and inflammatory mediators contribute to endothelial dysfunction in high-fat diet-induced obesity in mice. *Journal of Hypertension*, 28(10), 2111–2119. <https://doi.org/10.1097/HJH.0b013e32833ca68c>
- Koeberle, A., & Werz, O. (2015). Perspective of microsomal prostaglandin E2 synthase-1 as drug target in inflammation-related disorders. *Biochemical Pharmacology*, 98(1), 1–15. <https://doi.org/10.1016/j.bcp.2015.06.022>
- Leiguez, E., Motta, P., Maia Marques, R., Lomonte, B., Sampaio, S. V., & Teixeira, C. (2020). A representative GIIA phospholipase A₂ activates preadipocytes to produce inflammatory mediators implicated in

- obesity development. *Biomolecules*, 10(12), 1593. <https://doi.org/10.3390/biom10121593>
- Lilley, E., Stanford, S. C., Kendall, D. E., Alexander, S., Cirino, G., Docherty, J. R., George, C. H., Insel, P. A., Izzo, A. A., Ji, Y., Panettieri, R. A., Sobey, C. G., Stefanska, B., Stephens, G., Teixeira, M., & Ahluwalia, A. (2020). ARRIVE 2.0 and the *British Journal of Pharmacology*: Updated guidance for 2020. *British Journal of Pharmacology*, 177(16), 3611–3616. <https://doi.org/10.1111/bph.15178>
- Majewski, M., Jurgoński, A., Fotschki, B., & Juśkiewicz, J. (2018). The toxic effects of monosodium glutamate (MSG)—The involvement of nitric oxide, prostanoids and potassium channels in the reactivity of thoracic arteries in MSG-obese rats. *Toxicology and Applied Pharmacology*, 359, 62–69. <https://doi.org/10.1016/j.taap.2018.09.016>
- Mancia, G., Fagard, R., Narkiewicz, K., Redón, J., Zanchetti, A., Böhm, M., Christiaens, T., Cifkova, R., De Backer, G., Dominiczak, A., Galderisi, M., Grobbee, D. E., Jaarsma, T., Kirchhof, P., Kjeldsen, S. E., Laurent, S., Manolis, A. J., Nilsson, P. M., Ruilope, L. M., ... Task Force Members. (2013). 2013 ESH/ESC guidelines for the management of arterial hypertension: The task force for the management of arterial hypertension of the European Society of Hypertension (ESH) and of the European Society of Cardiology (ESC). *Journal of Hypertension*, 31(7), 1281–1357. <https://doi.org/10.1097/01.hjh.0000431740.32696.cc>
- Martínez-Martínez, E., López-Ándres, N., Jurado-López, R., Rousseau, E., Bartolomé, M. V., Fernández-Celis, A., Rossignol, P., Islas, F., Antequera, A., Prieto, S., Luaces, M., & Cachafeiro, V. (2015). Galectin-3 participates in cardiovascular remodeling associated with obesity. *Hypertension (Dallas, Tex.: 1979)*, 66(5), 961–969.
- Muñoz, M., Sánchez, A., Pilar Martínez, M., Benedito, S., López-Oliva, M. E., García-Sacristán, A., Hernández, M., & Prieto, D. (2015). COX-2 is involved in vascular oxidative stress and endothelial dysfunction of renal interlobar arteries from obese Zucker rats. *Free Radical Biology & Medicine*, 84, 77–90. <https://doi.org/10.1016/j.freeradbiomed.2015.03.024>
- Ozen, G., Gomez, I., Daci, A., Deschildre, C., Boubaya, L., Teskin, O., Uydeş-Doğan, B. S., Jakobsson, P.-J., Longrois, D., Topal, G., & Norel, X. (2017). Inhibition of microsomal PGE synthase-1 reduces human vascular tone by increasing PGI₂: A safer alternative to COX-2 inhibition. *British Journal of Pharmacology*, 174(22), 4087–4098. <https://doi.org/10.1111/bph.13939>
- Parlee, S. D., Lentz, S. I., Mori, H., & MacDougald, O. A. (2014). Quantifying size and number of adipocytes in adipose tissue. *Methods in Enzymology*, 537, 93–122. <https://doi.org/10.1016/B978-0-12-411619-1.00006-9>
- Percie du Sert, N., Hurst, V., Ahluwalia, A., Alam, S., Avey, M. T., Baker, M., Browne, W. J., Clark, A., Cuthill, I. C., Dirnagl, U., Emerson, M., Garner, P., Holgate, S. T., Howells, D. W., Karp, N. A., Lázic, S. E., Lidster, K., MacCallum, C. J., Macleod, M., ... Würbel, H. (2020). The ARRIVE guidelines 2.0: Updated guidelines for reporting animal research. *PLoS Biology*, 18(7), e3000410. <https://doi.org/10.1371/journal.pbio.3000410>
- Petersen, M. C., & Shulman, G. I. (2018). Mechanisms of insulin action and insulin resistance. *Physiological Reviews*, 98(4), 2133–2223. <https://doi.org/10.1152/physrev.00063.2017>
- Pierre, C., Guillebaud, F., Airault, C., Baril, N., Barbouche, R., Save, E., Gaigé, S., Bariouh, B., Dallaporta, M., & Troadec, J. D. (2018). Invalidation of microsomal prostaglandin E synthase-1 (mPGES-1) reduces diet-induced low-grade inflammation and adiposity. *Frontiers in Physiology*, 9, 1358. <https://doi.org/10.3389/fphys.2018.01358>
- Prieto, D., Contreras, C., & Sánchez, A. (2014). Endothelial dysfunction, obesity and insulin resistance. *Current Vascular Pharmacology*, 12(3), 412–426. <https://doi.org/10.2174/1570161112666140423221008>
- Riant, E., Waget, A., Cogo, H., Arnal, J. F., Burcelin, R., & Gourdy, P. (2009). Estrogens protect against high-fat diet-induced insulin resistance and glucose intolerance in mice. *Endocrinology*, 150(5), 2109–2117. <https://doi.org/10.1210/en.2008-0971>
- Samuelsson, B., Morgenstern, R., & Jakobsson, P. J. (2007). Membrane prostaglandin E synthase-1: A novel therapeutic target. *Pharmacological Reviews*, 59(3), 207–224. <https://doi.org/10.1124/pr.59.3.1>
- Sasaki, Y., Kuwata, H., Akatsu, M., Yamakawa, Y., Ochiai, T., Yoda, E., Nakatani, Y., Yokoyama, C., & Hara, S. (2021). Involvement of prostacyclin synthase in high-fat-diet-induced obesity. *Prostaglandins and Other Lipid Mediators*, 153, 106523. <https://doi.org/10.1016/j.prostaglandins.2020.106523>
- Stern, J. H., Rutkowski, J. M., & Scherer, P. E. (2016). Adiponectin, leptin, and fatty acids in the maintenance of metabolic homeostasis through adipose tissue crosstalk. *Cell Metabolism*, 23(5), 770–784. <https://doi.org/10.1016/j.cmet.2016.04.011>
- Touboul, P. J., Hennerici, M. G., Meairs, S., Adams, H., Amarenco, P., Bornstein, N., Csiba, L., Desvarieux, M., Ebrahim, S., Hernandez, R. H., Jaff, M., Kownator, S., Naqvi, T., Prati, P., Rundek, T., Sitzer, M., Schminke, U., Tardif, J.-C., Taylor, A., ... Woo, K. S. (2012). Mannheim carotid intima-media thickness and plaque consensus (2004–2006–2011). An update on behalf of the advisory board of the 3rd, 4th and 5th watching the risk symposia, at the 13th, 15th and 20th European Stroke Conferences, Mannheim, Germany, 2004, Brussels, Belgium, 2006, and Hamburg, Germany, 2011. *Cerebrovascular Diseases (Basel, Switzerland)*, 34(4), 290–296. <https://doi.org/10.1159/000343145>
- Vecchié, A., Dallegrì, F., Carbone, F., Bonaventura, A., Liberale, L., Portincasa, P., Frühbeck, G., & Montecucco, F. (2018). Obesity phenotypes and their paradoxical association with cardiovascular diseases. *European Journal of Internal Medicine*, 48, 6–17. <https://doi.org/10.1016/j.ejim.2017.10.020>
- Vessièrès, E., Belin de Chantemèrè, E. J., Toutain, B., Guihot, A. L., Jardel, A., Loufrani, L., & Henrion, D. (2010). Cyclooxygenase-2 inhibition restored endothelium-mediated relaxation in old obese Zucker rat mesenteric arteries. *Frontiers in Physiology*, 1, 145. <https://doi.org/10.3389/fphys.2010.00145>
- Wang, C. Y., & Liao, J. K. (2012). A mouse model of diet-induced obesity and insulin resistance. *Methods in Molecular Biology (Clifton, N.J.)*, 821, 421–433. https://doi.org/10.1007/978-1-61779-430-8_27
- Wang, M., Ihida-Stansbury, K., Kothapalli, D., Tamby, M. C., Yu, Z., Chen, L., Grant, G., Cheng, Y., Lawson, J. A., Assoian, R. K., Jones, P. L., & FitzGerald, G. A. (2011). Microsomal prostaglandin e2 synthase-1 modulates the response to vascular injury. *Circulation*, 123(6), 631–639. <https://doi.org/10.1161/CIRCULATIONAHA.110.973685>
- Wang, M., Lee, E., Song, W., Ricciotti, E., Rader, D. J., Lawson, J. A., Puré, E., & FitzGerald, G. A. (2008). Microsomal prostaglandin E synthase-1 deletion suppresses oxidative stress and angiotensin II-induced abdominal aortic aneurysm formation. *Circulation*, 117(10), 1302–1309. <https://doi.org/10.1161/CIRCULATIONAHA.107.731398>
- Wang, M., Zukas, A. M., Hui, Y., Ricciotti, E., Puré, E., & FitzGerald, G. A. (2006). Deletion of microsomal prostaglandin E synthase-1 augments prostacyclin and retards atherogenesis. *Proceedings of the National Academy of Sciences of the United States of America*, 103(39), 14507–14512. <https://doi.org/10.1073/pnas.0606586103>
- Wu, D., Mennerich, D., Arndt, K., Sugiyama, K., Ozaki, N., Schwarz, K., Wei, J., Wu, H., Bishopric, N. H., & Doods, H. (2009). Comparison of microsomal prostaglandin E synthase-1 deletion and COX-2 inhibition in acute cardiac ischemia in mice. *Prostaglandins & Other Lipid Mediators*, 90(1–2), 21–25. <https://doi.org/10.1016/j.prostaglandins.2009.06.006>

Zhu, L., Xu, C., Huo, X., Hao, H., Wan, Q., Chen, H., Zhang, X., Breyer, R. M., Huang, Y., Cao, X., Liu, D. P., FitzGerald, G. A., & Wang, M. (2019). The cyclooxygenase-1/mPGES-1/endothelial prostaglandin EP4 receptor pathway constrains myocardial ischemia-reperfusion injury. *Nature Communications*, 10(1), 1888. <https://doi.org/10.1038/s41467-019-09492-4>

SUPPORTING INFORMATION

Additional supporting information may be found in the online version of the article at the publisher's website.

How to cite this article: Ballesteros-Martínez, C., Rodrigues-Díez, R., Beltrán, L. M., Moreno-Carriles, R., Martínez-Martínez, E., González-Amor, M., Martínez-González, J., Rodríguez, C., Cachofeiro, V., Salaices, M., & Briones, A. M. (2022). Microsomal prostaglandin E synthase-1 is involved in the metabolic and cardiovascular alterations associated with obesity. *British Journal of Pharmacology*, 179(11), 2733–2753. <https://doi.org/10.1111/bph.15776>